2017

A photosynthesis-based two-leaf canopy stomatal conductance model for meteorology and air quality modeling with WRF/CMAQ PX LSM

Limei Ran
United States Environmental Protection Agency, ran.limei@eap.gov

Jonathan Pleim
United States Environmental Protection Agency

Conghe Song
University of North Carolina at Chapel Hill

Larry Band
University of North Carolina at Chapel Hill

John T. Walker
United States Environmental Protection Agency

See next page for additional authors

AGU PUBLICATIONS

JGR

Journal of Geophysical Research: Atmospheres

RESEARCH ARTICLE
10.1002/2016JD025583

Key Points:
- A coupled photosynthesis-stomatal conductance model is implemented and evaluated for PX LSM in WRF/CMAQ
- The photosynthesis-based model simulates latent heat as well as the current Jarvis functional approach in PX LSM
- The photosynthesis-based model shows distinct advantages in simulating LH and ozone fluxes for grassland

Correspondence to:
L. Ran,
Ran.Limei@eap.gov

Citation:
Ran, L., J. Pleim, C. Song, L. Band, J. T. Walker, and F. S. Binkowski (2017), A photosynthesis-based two-leaf canopy stomatal conductance model for meteorology and air quality modeling with WRF/CMAQ PX LSM, *J. Geophys. Res. Atmos.*, *122*, doi:10.1002/2016JD025583.

Received 28 JUN 2016
Accepted 19 DEC 2016
Accepted article online 22 DEC 2016

A photosynthesis-based two-leaf canopy stomatal conductance model for meteorology and air quality modeling with WRF/CMAQ PX LSM

Limei Ran[1], Jonathan Pleim[1], Conghe Song[2], Larry Band[2,3], John T. Walker[1], and Francis S. Binkowski[3]

[1]United States Environmental Protection Agency, Research Triangle Park, North Carolina, USA, [2]Department of Geography, University of North Carolina at Chapel Hill, Chapel Hill, North Carolina, USA, [3]Institute for the Environment, University of North Carolina at Chapel Hill, Chapel Hill, North Carolina, USA

Abstract A coupled photosynthesis-stomatal conductance model with single-layer sunlit and shaded leaf canopy scaling is implemented and evaluated in a diagnostic box model with the Pleim-Xiu land surface model (PX LSM) and ozone deposition model components taken directly from the meteorology and air quality modeling system—WRF/CMAQ (Weather Research and Forecast model and Community Multiscale Air Quality model). The photosynthesis-based model for PX LSM (PX PSN) is evaluated at a FLUXNET site for implementation against different parameterizations and the current PX LSM approach with a simple Jarvis function (PX Jarvis). Latent heat flux (LH) from PX PSN is further evaluated at five FLUXNET sites with different vegetation types and landscape characteristics. Simulated ozone deposition and flux from PX PSN are evaluated at one of the sites with ozone flux measurements. Overall, the PX PSN simulates LH as well as the PX Jarvis approach. The PX PSN, however, shows distinct advantages over the PX Jarvis approach for grassland that likely result from its treatment of C_3 and C_4 plants for CO_2 assimilation. Simulations using Moderate Resolution Imaging Spectroradiometer (MODIS) leaf area index (LAI) rather than LAI measured at each site assess how the model would perform with grid averaged data used in WRF/CMAQ. MODIS LAI estimates degrade model performance at all sites but one site having exceptionally old and tall trees. Ozone deposition velocity and ozone flux along with LH are simulated especially well by the PX PSN compared to significant overestimation by the PX Jarvis for a grassland site.

1. Introduction

The combined meteorology and air quality modeling system, composed of the Weather Research and Forecast (WRF) model [*Skamarock et al*., 2008] and Community Multiscale Air Quality (CMAQ) model [*Byun and Schere*, 2006] is an important tool that increases our understanding of the chemical and physical processes contributing to air quality impairment and facilitates the development of policies to mitigate harmful effects of air pollution on human health and the environment around the world [e.g., *Cohan et al*., 2007; *Wang et al*., 2010; *Compton et al*., 2011; *Hogrefe et al*., 2015; *Xing et al*., 2015]. In spite of significant advancements in model performance over the past decade, improvements are still needed [*Foley et al*., 2010; *Appel et al*., 2011]. For example, WRF/CMAQ tends to overestimate ozone (O_3) in the southeastern and Gulf of Mexico regions of the United States (U.S.), while O_3 estimates in the northern U.S. agree well with observations. The recent study by *Ran et al*. [2016] shows the model's persistent tendency to overestimate O_3 in these regions (Figure 1). Many components from this complex modeling system including emissions, transport, photochemistry, and land surface exchange may contribute to these errors. This research focuses on advancing land surface model (LSM) meteorological (heat, moisture, and momentum) and chemical (dry deposition and bidirectional exchange) surface flux processes in the WRF/CMAQ system by reducing uncertainty associated with the simulation of vegetation processes.

Plants open their stomata to obtain atmospheric carbon dioxide for photosynthesis while at the same time they lose water because of the diffusion of water molecules from leaf chloroplasts to the atmosphere. An important function of LSMs is to model stomatal conductance for estimating evapotranspiration (ET) which includes leaf transpiration and evaporation from soil pores, plant litters, open water bodies, and leaf cuticle surfaces [*Bonan*, 2008]. The Pleim-Xiu (PX) [*Pleim and Xiu*, 1995; *Xiu and Pleim*, 2001] and Noah [*Chen and Dudhia*, 2001] LSMs are two of WRF LSMs which are commonly used for mesoscale meteorology simulations. The PX LSM is particularly designed for air quality applications using the CMAQ model [e.g., *Eder*

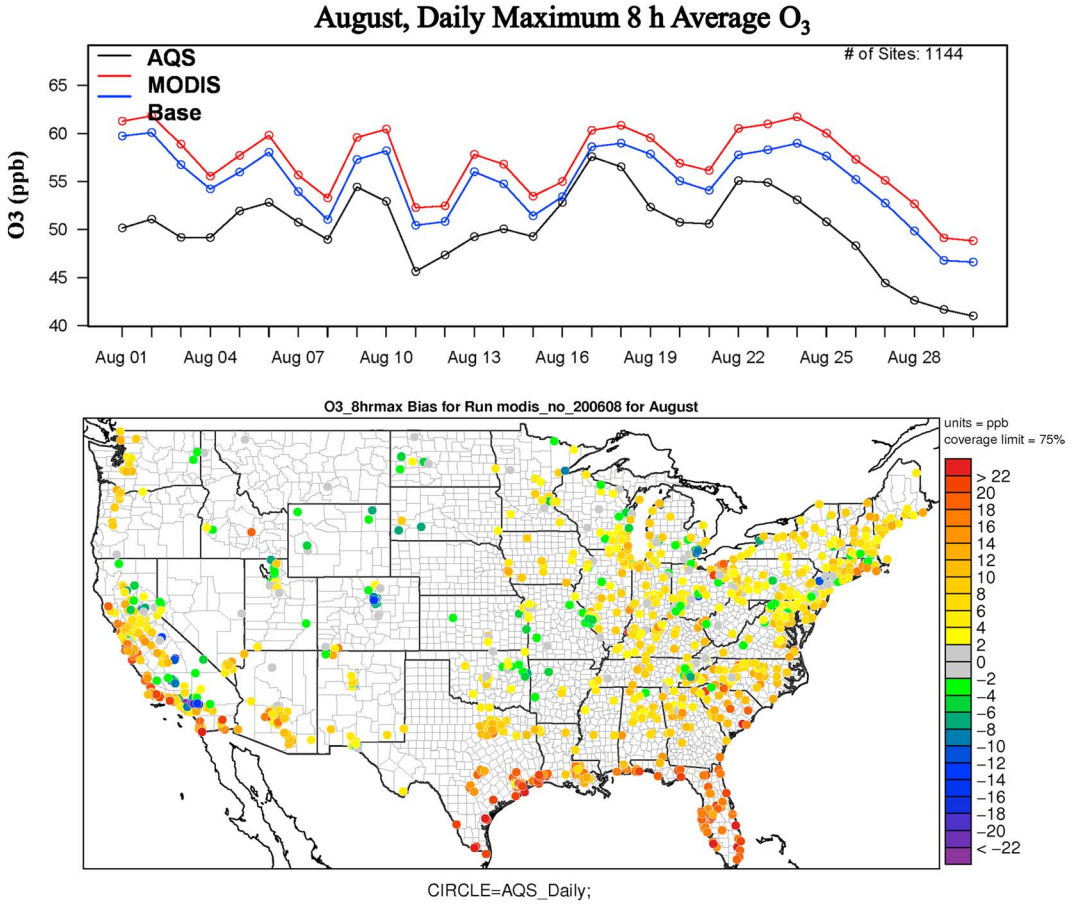

Figure 1. Evaluation of August 2006 daily maximum 8 h average O_3 (ppb) simulated from an improved WRF/CMAQ with/without (base) MODIS vegetation and albedo input against the U.S. Environmental Protection Agency Air Quality System (AQS) sites. (top) Mean of daily maximum 8 h average O_3 from the base model (blue line), the model with MODIS input (red line), and all AQS sites (black line). (bottom) The mean bias for daily maximum 8 h average O_3 simulated from WRF/CMAQ without MODIS input. The base model's vegetation is computed from vegetation parameters prescribed in land use category lookup tables using equations (2) and (3) in *Ran et al.* [2015].

et al., 2009; *Kelly et al.*, 2014; *Hogrefe et al.*, 2015], which uses parameters such as stomatal and aerodynamic resistances directly from the PX LSM in its dry deposition calculations [*Pleim and Ran*, 2011]. Similarly, the CMAQ model uses the same planetary boundary layer (PBL) model, the Asymmetric Convective Model version 2 [*Pleim*, 2007a, 2007b], that can be consistently configured in WRF. Unlike climate LSMs [e.g., *Oleson et al.*, 2013; *Clark et al.*, 2011] with complex hydrology and dynamic vegetation coupled with climate to model processes over decadal to century future periods, the PX and Noah LSMs have relatively simple prognostic soil water models (PX has two soil layers and Noah has four) which rely heavily on data initialization and assimilation for high accuracy over relatively short periods (days to years). Both the LSMs have simple canopy treatments with a big leaf empirical stomatal conductance function following the approach described by *Noilhan and Planton* [1989] in the Interactions Soil Biosphere Atmosphere (ISBA) LSM. Surface characteristics including vegetation parameters and surface albedo are specified in LSM land use lookup tables, and plant phenological dynamics are modeled using simple time and deep soil temperature dependent functions. With increasing needs to conduct year-long retrospective WRF/CMAQ simulations, LSMs using simple canopy treatment with table-prescribed surface representations clearly show limitations in capturing seasonal landscape changes and disturbances. In addition, lacking a biochemically based photosynthesis-conductance scheme could limit not only the model's dynamic responses to environmental conditions such as temperature, air pollutants (e.g., O_3), and CO_2 concentration but also their applications in assessing the coupling effects of air quality and vegetation productivity in changing climate.

There are ongoing efforts to improve the land surface processes in WRF/CMAQ with the PX LSM option. For instance, the high-resolution 30 m National Land Cover Database (NLCD) as well as Moderate Resolution Imaging Spectroradiometer (MODIS) 500 m land cover data are used in the system [*Pleim and Ran*, 2011]. There are recent improvements to the vegetation, soil, and PBL processes [*Pleim et al*., 2016]. *Ran et al*. [2015, 2016] incorporated MODIS vegetation and albedo products in the system, and they conclude that realistic vegetation characteristics and phenology from MODIS products help improve the 2 m mixing ratio (Q) simulation during the growing season. This research furthers their study through enhancing the vegetation model using a photosynthesis-based stomatal physiology process approach which is commonly used in Earth system models [*Bonan et al*., 2011; *Clark et al*., 2011; *Kowalczyk et al*., 2013; *Oleson et al*., 2013]. Incorporating the impacts of CO_2 in WRF/CMAQ through using a photosynthesis-based approach will be an important advance in the modeling capabilities which will allow the model to respond to changing CO_2 levels in space and time.

The objective of the study is to implement a coupled leaf photosynthesis and stomatal conductance approach in PX LSM for meteorology and air quality modeling with MODIS vegetation input. This paper focuses on the implementation and evaluation of the photosynthesis-based approach in a diagnostic box model with the PX LSM and CMAQ dry deposition model components that are directly from the updated WRF/CMAQ system presented by *Ran et al*. [2016]. The questions which the paper addresses are (i) how does the PX LSM with a coupled leaf photosynthesis and stomatal conductance approach influence the performance of latent heat (LH) flux and ozone dry deposition and, (ii) can the photosynthesis approach better represent diurnal variations in LH flux and ozone dry deposition than the current approach, and (iii) how does the photosynthesis approach combined with MODIS leaf area index (LAI) influence LH fluxes?

The coupled photosynthesis-conductance model, ozone deposition and flux computation, and model implementation are described in section 2. Section 3 first presents the model evaluation at the FLUXNET Harvard Forest US-Ha1 site which is used for implementation. Next, further evaluation and analyses of the photosynthesis-based approach are described compared to measurements from four selected FLUXNET sites (Missouri Ozark/US-MOz, Wind River Field Station/US-Wrc, Fermi Prairie/US-IB2, and Mead Irrigated Rotation/US-Ne2) which have different vegetation types and to ozone and surface flux measurements by the U.S. Environmental Protection Agency (EPA) at the Duke Forest Open Field site in North Carolina. MODIS vegetation input to the diagnostic box model is also evaluated to demonstrate the advantages and limitations in using MODIS input to the advanced PX LSM. MODIS LAI is evaluated against observed LAI which are available at the selected FLUXNET measurement sites. Conclusions and future work are presented in the last section.

2. Photosynthesis-Based Stomatal Conductance Approach

Vegetation plays an important role not only in the surface energy budget but also in water and carbon cycles [*Jarvis and McNaughton*, 1986; *Bonan*, 2008; *Katul et al*., 2012]. In addition, vegetation can act as both a source and a sink of atmospheric gas-phase chemical species including CO_2, O_3, NH_3, NO_2, SO_2, and a wide array of volatile organic compounds. A key function of LSMs is to estimate LH flux (λE), which is the product of the latent heat of vaporization (λ) times evaporative water flux (E, also called evapotranspiration—ET). ET includes leaf transpiration and water evaporation from soil, litter and vegetation surfaces and open water bodies [*Bonan*, 2008]. During the growing season, transpiration is often dominant in controlling ET from vegetated lands [*Budyko*, 1974]. Stomata control the amount of water transpired by vegetation so that stomatal conductance and its scaling from leaf to canopy are key processes in estimating ET. Following approaches developed for global climate models (GCMs) [*Dai et al*., 2004; *Cox et al*., 1998; *Bonan et al*., 2011; *Clark et al*., 2011; *Kowalczyk et al*., 2013; *Oleson et al*., 2013] and ecosystem productivity models [*Campbell and Norman*, 1998; *Medlyn et al*., 2005; *Song et al*., 2009; *Evers et al*., 2010; *Baker et al*., 2010], we implemented a coupled photosynthesis-based stomatal conductance model with sunlit and shaded leaves in the PX LSM for coupling ET estimation with CO_2 assimilation.

2.1. Stomatal Conductance

The current PX LSM models canopy stomatal conductance (G_{st}) of gasses following the empirical multiplicative Jarvis approach [*Jarvis*, 1976] which assumes independent environmental functions. The PX LSM treats the

whole canopy as a single leaf (one-big leaf model). The canopy fluxes from the big leaf are calculated as the leaf-scale fluxes times the canopy LAI. Following the Jarvis approach presented in the ISBA LSM [*Noilhan and Planton*, 1989], with modifications for PX LSM [*Pleim and Xiu*, 1995], the canopy level conductance, G_{st}, is computed as

$$G_{st} = \mathrm{LAI}^{*}\left[\frac{1}{R_{stmin}} F_1(\mathrm{PAR}) F_2(w_2) F_3(\mathrm{RH}_s) F_4(T_{ic})\right] \tag{1}$$

where R_{stmin} is the minimum stomatal resistance for each land cover type specified in the LSM land cover lookup table. The functions F_{1-4}, which are defined by *Xiu and Pleim* [2001], represent the fractional degree (0 to 1) of stomatal closure caused by the environmental factors: photosynthetically active radiation (PAR), root-depth soil moisture (w_2), relative humidity at the leaf surface (RH_s), and air temperature in the canopy (T_{ic}). The influence of ambient CO_2 concentration on stomatal opening is not included in the current PX LSM with the assumption that the CO_2 concentration is constant for the relatively short period typically used for mesoscale meteorology simulations. The advantage of this simple empirical approach is that it can be easily implemented for large-scale simulations with a small set of vegetation parameters such as LAI and R_{stmin} and that it generally produces reasonable results for retrospective simulations with initial or real-time assimilated soil conditions [*Noilhan and Mahfouf*, 1996; *Chen and Dudhia*, 2001; *Xiu and Pleim*, 2001; *Gilliam and Pleim*, 2010]. The weakness of such simplistic models is that they depend on the limited number of multiplicative functions, which are related to environment variables that are often not actually independent. The multiplicative big leaf model does not depend on measurable physiological or physical parameters and must be calibrated using stand or canopy level eddy flux measurements. Although the big leaf model is simple and widely used in many disciplines, it is often criticized for ignoring canopy gradients and differences between plant and soil components within the canopy [*Jarvis*, 1995; *de Pury and Farquhar*, 1997; *Wang and Leuning*, 1998].

The stomatal conductance (g_{st}) at the leaf scale in the photosynthesis-based PX LSM is modeled after the widely used Ball-Woodrow-Berry (BWB) approach [*Ball et al*., 1987], which relates g_{st} directly to net CO_2 assimilation rate (A_{net}) based on plant physiological processes. g_{st} is modeled in the PX LSM following the semiempirical BWB model described by *Collatz et al*. [1991, 1992], applied in a GCM by *Sellers et al*. [1996], and implemented in the Community Land Model version 4 (CLM4.5) [*Bonan et al*., 2011; *Oleson et al*., 2013] within the Community Earth System Model as

$$g_{st} = g_0 + m_g \frac{A_{net}}{c_s} \frac{e_s}{e_i} P_a \tag{2}$$

where g_0 is set to 0.01 mol m^{-2} s^{-1} for C_3 plants and 0.04 mol m^{-2} s^{-1} for C_4 plants, m_g is a plant-type parameter which is 9 for C_3 plants and 4 for C_4 plants, c_s is the CO_2 partial pressure at the leaf surface, e_s is the vapor pressure at the leaf surface, e_i is the saturation vapor pressure inside the leaf stomata at the vegetation surface temperature (T_s), and P_a is the atmospheric pressure. Soil moisture stress is considered similar to the PX Jarvis LSM, where the empirical function F_2 (equation (3)) is used to scale canopy stomatal conductance and net CO_2 assimilation rate following the approach used by the Joint UK Land Environment Simulator (JULES) LSM model [*Clark et al*., 2011]. The function F_2 with a relatively smooth S shape that is very similar to the JULES soil stress factor is computed as

$$F_2 = \frac{1}{1 + \exp\{-5[w_{2avl}/w_{2mxav} - (w_{2mxav}/3 + w_{wlt})]\}} \tag{3}$$

with

$$w_{2avl} = w_2 - w_{wlt}, \quad w_{2mxav} = w_{fc} - w_{wlt}$$

where w_{fc} is the volumetric water content at field capacity and w_{wlt} is the wilting point.

2.2. Leaf-Scale Photosynthesis

The new PX LSM formulation defines the net CO_2 assimilation rate, A_{net}, of C_3 and C_4 plants at the leaf scale based on the biochemical model of photosynthesis described by *Farquhar et al*. [1980]. GCMs [*Clark et al*., 2011; *Bonan et al*., 2011] and land surface exchange studies [*Song et al*., 2009; *Evers et al*., 2010] commonly employ this approach when modeling plant transpiration and productivity. The CO_2 assimilation rate (A) is calculated based on colimitation among three potential assimilation rates [*Bonan et al*., 2011]: limited by Rubisco (nitrogen related, A_c), light (photon related, A_j), and transport of photosynthetic products for C_3

plants and phosphoenolpyruvate (PEP) carboxylase limitation for C_4 plants (A_e). A_{net} (mol CO_2 m^{-2} s^{-1}) is then obtained by excluding leaf dark respiration from A following JULES (Appendix A).

2.3. Leaf to Canopy Scaling

Upscaling the coupled CO_2 assimilation rate and stomatal conductance from the leaf to canopy is complicated by spatial heterogeneity within plant canopies in both the vertical and horizontal dimensions. LAI [*Chen et al*., 2006], leaf inclination angles and leaf clumping [*Pisek et al*., 2013], crown gappiness [*Song et al*., 2009], leaf nitrogen, and photosynthetic capacity [*Leuning et al*., 1995; *Baldocchi and Meyers*, 1998] vary within the canopy, collectively affecting canopy transpiration, CO_2 assimilation, and other flux processes. In addition, the nonlinearity of key physiological and physical processes such as leaf photosynthesis and transpiration with many abiotic regulating variables (e.g., solar and terrestrial radiation, temperature, humidity, wind speed, and soil moisture) further complicates the difficulty in upscaling those processes [*Campbell and Norman*, 1998]. Leaf stomatal conductance in a canopy can be quite different at different locations due to both current and past-varying abiotic and biotic conditions (e.g., age and height). Because of this complication, modeling and validating parameterized processes that govern land surface fluxes across different time and space scales remain challenging [*Moorcroft*, 2006]. Scaling methods from the leaf to canopy vary with different complexity from the simplest one-big leaf models [*Monteith*, 1981; *Jarvis*, 1995; *Pleim and Xiu*, 1995; *Chen and Dudhia*, 2001] to two-big leaf models [*de Pury and Farquhar*, 1997; *Wang and Leuning*, 1998] and multilayer models [*Meyers et al*., 1998; *Kobayashi et al*., 2012]. A weakness of one-big leaf models is that they treat sunlit and shaded leaves within the canopy equally. This equal treatment of the canopy leaves often results in overestimation of flux rates (e.g., CO_2) [*de Pury and Farquhar*, 1997; *Wang and Leuning*, 1998]. The sunlit and shaded leaves have distinct differences in leaf surface temperature, which results in different surface vapor pressure. Thus, stomata will behave differently under varying micrometeorological conditions within the canopy. *de Pury and Farquhar* [1997] and *Wang and Leuning* [1998] demonstrated that a single-layer sunlit/shaded big leaf model is simpler but has equivalent predictive capabilities for CO_2 assimilation rate and LH as a multilayer model. *Zhang et al*. [2001] also showed that the sunlit/shaded big leaf approach compares well to multilayer models for representing the stomatal pathway in dry deposition models. For the mesoscale modeling purpose, the photosynthesis-based PX LSM model also adopts the sunlit (LAI_{sun}) and shaded (LAI_{shd}) two-big leaf approach for canopy scaling (Appendix B).

The canopy stomatal conductance (G_{st}) and net CO_2 assimilation rate (A_{cnet}) with the soil moisture constraint are computed as

$$G_{st} = (g_{st\_sun} \times LAI_{sun} + g_{st\_shd} \times LAI_{shd}) F_2 \tag{4}$$

$$A_{cnet} = (A_{net\_sun} \times LAI_{sun} + A_{net\_shd} \times LAI_{shd}) F_2 \tag{5}$$

where g_{st_sun}/g_{st_shd} (m s^{-1}) and A_{net_sun}/A_{net_shd} (mol m^{-2} s^{-1}) are computed leaf-scale stomatal conductance and net CO_2 assimilation rate for the sunlit and shaded leaves. The transpiration from the sunlit or shaded canopy leaf (TR_{c_sun} or TR_{c_shd}), with the soil moisture constraint on the stomatal conductance, is computed following the PX LSM approach as

$$TR_{c\_sun} = \rho_{air} \frac{q_{s(T_{s\_sun})} - q_a}{R_{bw} + R_a + 1/(LAI_{sun} \times g_{stw\_sun} \times F_2)} \tag{6}$$

where ρ_{air} is the air density (kg m^{-3}), $q_{s(Ts\_sun)}$ is the saturated mixing ratio for water vapor at the sunlit leaf temperature T_{s_sun}, q_a is the ambient water vapor mixing ratio above the canopy, R_{bw} is the quasi-laminar boundary layer resistance for water (m s^{-1}), R_a is the air dynamic resistance (m s^{-1}), and g_{stw_sun} is the sunlit leaf stomatal conductance for water (m s^{-1}) computed from g_{st} (equation (2)) for CO_2. The transpiration for the shaded leaf is computed using the same equation but with parameters for the shaded leaf. The transpiration (TR_c) for the whole canopy is then computed as

$$TR_c = TR_{c\_sun} + TR_{c\_shd} \tag{7}$$

The evapotranspiration (ET_c) for the canopy is computed as

$$ET_c = TR_c + E_{ss} + E_{vs} \tag{8}$$

where E_{ss} and E_{vs} are the evaporation from the bare soil surface and vegetation surface and they are

estimated based on the current PX LSM approach [*Pleim and Xiu*, 1995; *Ran et al*., 2016]. Both the photosynthesis-based model and current PX approach use the same estimated E_{ss} and E_{vs} in ET computation. Thus, the comparison of LH between the two approaches purely reflects the differences in modeled plant transpiration.

2.4. Ozone Dry Deposition

Dry deposition is an important sink for ozone in the atmosphere, while it also affects photosynthesis and stomatal conductance. Ozone dry deposition has a strong stomatal pathway in vegetated areas [*Wesely et al*., 1982; *Padro*, 1996]. The O_3 dry deposition flux (F_{O3}) can be estimated as the product of dry deposition velocity (V_d) and O_3 concentration near the ground (C_{O3}) [*Wesely and Hicks*, 2000]:

$$F_{O3} = V_d C_{O3} \tag{9}$$

The box model calculations of O_3 flux follow the CMAQ approach described by *Pleim and Ran* [2011]. Because of its strong stomatal pathway, the CMAQ dry deposition model is designed to use the same aerodynamic and canopy stomatal conductance (adjusted by the ratio of O_3 diffusivity to water vapor diffusivity) estimated in WRF with the PX LSM for ET computation [*Pleim et al*., 2001]. Thus, stomatal conductance calculated by the photosynthesis approach will influence the estimation of the ozone flux and further affect modeled surface ozone concentration. The ozone dry deposition velocity is computed from resistances in series and parallel as

$$R_s = \left(\frac{1}{1/G_{st} + R_m} + \frac{1}{R_w} + \frac{1}{R_{ac} + R_g} \right)^{-1} \tag{10}$$

$$V_d = \frac{1}{R_a + R_{bO3} + R_s} \tag{11}$$

where R_s is the surface resistance, R_m is the leaf mesophyll resistance, R_w is the cuticular resistance, R_{ac} is the in-canopy resistance, R_g is the ground resistance, and R_{bO3} is the quasi-laminar boundary layer resistance for ozone. The modeled O_3 deposition flux and dry deposition velocity are compared to the measurements made by eddy correlation at the Duke Forest Open Field grassland site as described by *Almand-Hunter et al*. [2015].

2.5. Box Model Implementation

The coupled photosynthesis and stomatal conductance (PX-PSN) approach is implemented in a diagnostic box model with the ET and ozone deposition velocity routines from WRF/CMAQ with PX LSM described by *Ran et al*. [2016]. This box model is designed to use as many observational data as possible from the FLUXNET L2 standardized data [*Baldocchi*, 2008] for evaluating modeled LH and ozone fluxes from the PX PSN and current Jarvis approach (PX Jarvis) in comparison with observations. Since the box model is diagnostic and there is no energy budget calculation, observed sensible heat is used to compute aerodynamic surface temperature, which is used as the leaf temperature in the PX Jarvis. Observed friction velocity (u_*) is used to compute the boundary layer resistance and aerodynamic resistance based on the Monin-Obukov similarity theory (MOST) [*Monin and Obukhov*, 1954; *Oleson et al*., 2013; *Pleim and Ran*, 2011]. The computed aerodynamic surface temperature is not used in the PX PSN, which estimates the sunlit and shaded leaf surface temperatures using the net radiation on each leaf. Thus, the PX Jarvis may have some advantage in these box model experiments by using more observed data in simulations than the PX PSN. The observed air temperature, wind speed, LH, PAR, soil moisture, ambient CO_2 concentration, relative humidity, vapor pressure deficit, air pressure, precipitation, and LAI (if available) are input to the box model. To solve the equations for each sunlit and shaded leaf, an iterative numerical scheme, similar to CLM4.5 [*Oleson et al*., 2013], is used to estimate the leaf surface CO_2 partial pressure (c_s), g_{st}, A_{net}, and CO_2 partial pressure inside the leaf stomata (c_i) until c_i converges. At the same time, the leaf temperature is also numerically iterated outside the c_i iteration using the Penman-Monteith equation with R_{net} for each leaf.

3. Model Evaluation and Analysis

The PX PSN is implemented based on the 2006 flux measurements from the FLUXNET Harvard Forest US-Ha1 site. The performance of the model is first evaluated against the measurement data from the site used for the model implementation. The model is further evaluated and analyzed for LH estimation at four selected

FLUXNET sites with different vegetation types and landscape characteristics. The evaluation is conducted over the period with FLUXNET LAI measurements for each site, and LAI is linearly interpolated for the days in between LAI observations. Additional model simulations are made using the 2006 gap-filled MODIS vegetation data processed for each land cover type within a WRF/CMAQ 12 km grid cell to show the model performance and limitations when using the averaged MODIS vegetation for each plant function type (PFT) within a grid cell for typical mesoscale applications. The gap-filled MODIS LAI data are processed from 2006 MODIS Collection 5 LAI and FPAR data (MOD15A2GFS) at 1 km resolution and every 8 days [*Gao et al*., 2008; *Myneni et al*., 2011] from the North American Carbon Program as used in the previous studies by *Ran et al*. [2015, 2016]. The model is further evaluated based on the 2013 measurements at the Duke Forest Open Field-US-Dk1, made by U.S. EPA [*Almand-Hunter et al*., 2015], to assess the impact of the photosynthesis-based approach on LH, ozone deposition velocity, and ozone flux. Site descriptions; key parameters adopted from CLM4.5 [*Oleson et al*., 2013], JULES [*Clark et al*., 2011], and PX LSM [*Xiu and Pleim*, 2001; *Pleim et al*., 2013] based on site PFT and soil type; and simulation year for the five measurement sites are presented in Table 1. There are two soil moisture measurements at two different depths available in the FLUXNET Level 2 (L2) standardized file. However, some sites, such as Harvard forest, report no soil moisture measurements at all. Depending on the season, the model responds to the two soil moisture measurements differently, as plants tend to use shallow water with more nutrients when there is no water stress, but tap into deeper soil water when the upper layers are dry during the hot summer. Interpolated soil water between the two measurements generally requires that it be weighted by root distribution before model performance improvement is noted. Therefore, the model uses the soil moisture measurement which fits model performance best for the simulation periods at each site.

Estimated fluxes are evaluated using diurnal median comparisons between the two approaches against observations. In addition, the two approaches are evaluated using scatterplots of daily values of estimated fluxes (e.g., LH and O_3 flux) against observations with computed normalized mean bias (NMB) and normalized mean error (NME) from daily flux estimations. The NMB and NME metrics for model estimations are calculated as [e.g., *Yu et al*., 2006]

$$\mathrm{NMB} = \frac{\Sigma(M_i - O_i)}{\Sigma O_i} \times 100 \tag{12}$$

$$\mathrm{NME} = \frac{\Sigma|M_i - O_i|}{\Sigma O_i} \times 100 \tag{13}$$

where M_i and O_i are the estimated and observed daily total fluxes for day i. The two relative metrics in percent are useful to evaluate errors of modeling results against observations for fluxes which can have quite different magnitude and variability across the different sites.

3.1. Implementation Site Evaluation

The key parameters for canopy scaling and canopy radiative transfer are evaluated in Figure 2 based on the Harvard Forest US-Ha1 site data. The sunlit leaf is dominant at the lower LAI, while the shaded leaf increases with the increase of LAI (Figure 2 top left) for the assumed spherical leaf distribution of the broadleaf forest site. The sunlit leaf absorbs the majority of the incident PAR (Figure 2, top right) at the top of the canopy; the absorbed fraction peaks for LAI around 4 with a slightly decreasing trend following the increase of LAI due to the increase of shaded leaf LAI. The changes of the sunlit/shaded LAI and absorbed PAR fractions are very similar to the parameters displayed by *Bonan et al*. [2011]. With an assumed LAI at 4, most of the leaves are shaded and the sunlit leaf fraction is greatest at 0 solar zenith angle (Figure 2, bottom left). The shaded leaf LAI increases and the sunlit leaf LAI decreases with increasing zenith angle. The direct beam extinction coefficient (red line in Figure 2, bottom right) increases with the zenith angle exponentially (particularly after 80°) and is greater than 1 for zenith angles greater than 60°, which is consistent with *Campbell and Norman* [1998]. K_{dir} is limited to 3 in the model to avoid unstable numerical iteration without convergence. The diffuse beam extinction coefficient is a function of LAI (blue line in Figure 2, bottom right), and it decreases exponentially with the increase of LAI.

Figure 3 illustrates the influence of deep soil moisture on the stomatal conductance, net assimilation rate, and canopy transpiration (equations 4–6). The S shape function indicates that stomatal conductance, net CO_2 assimilation, and transpiration reach their potential values where the soil moisture is greater than field

Table 1. Site and Key Parameter Information for Flux Measurement Sites

Site Name	Vegetation and SiteInfo	Key Parameters
	FLUXNET Measurements	
2006 HarvardForest/US-Ha1	Deciduous broadleaf C3,location (−72.1715,42.5378), elevation 340 m, Massachusetts [*Urbanski et al*. 2007]	Canopy height = 25 m, OBS LAI, $x = 1$ (spherical leaf), α_{leaf} PAR = 0.8, α_{leaf} NIR = 0.2, forest floor reflectance = 0.10, $VCMAX25\_0 = 30 \times 10^{-6}$ mol m^{-2} s^{-1}, $kn = 0.17$, $Tlow = 0$°C, $Tup = 36$°C, leaf scattering coefficient 0.15,quantum yield $\varepsilon = 0.08$ (mol CO2[mol PAR photons]$^{-1}$), Jarvis $Rstmin = 200$ s m^{-1}, loam with $wsat = 0.451$, $wfc = 0.24$, $wwlt = 0.155$
2006 MissouriOzark/US-Moz	Deciduous broadleaf C3,location (−92.2, 38.7441),elevation 219 m, Missouri [*Gu et al*. 2006]	Canopy height = 24 m, OBS LAI, $x = 1$ (spherical leaf), α_{leaf} PAR = 0.8, α_{leaf} NIR = 0.2, forest floor reflectance = 0.10, $VCMAX25\_0 = 30 \times 10^{-6}$ mol m^{-2} s^{-1}, $kn = 0.17$, $Tlow = 0$°C, $Tup = 36$°C, leaf scattering coefficient 0.15,quantum yield $\varepsilon = 0.08$ (mol CO2[mol PAR photons]$^{-1}$), Jarvis $Rstmin = 200$ s m^{-1} (same as Harvard Forest US-Ha1 site), silt loam with $wsat = 0.485$, $wfc = 0.255$, $wwlt = 0.178$
2008 WindRiver Field Station/ US-Wrc	Evergreen needleleaf C3,location (−121.9519,45.8205), elevation 371 m, Washington [*Paw U et al*. 2004]	Canopy height = 56 m, LAI = 8.6, $x = 1$ (spherical leaf), α_{leaf} PAR = 0.8, α_{leaf} NIR = 0.2, forest floor reflectance = 0.10, $VCMAX25\_0 = 55 \times 10^{-6}$ mol m^{-2} s^{-1}, $kn = 0.17$, $Tlow = -10$°C, $Tup = 26$°C, leaf scattering coefficient 0.17, quantum yield $\varepsilon = 0.08$ (mol CO2[mol PAR photons]$^{-1}$), Jarvis $Rstmin = 175$ s m^{-1}, silt loam with $wsat = 0.485$, $wfc = 0.255$, $wwlt = 0.178$
2006 FermiPrairie/US-IB2	Grasslands C4,location (−88.241,41.8406), elevation 226m, Illinois [*Allison et al*. 2005]	Canopy height = 1 m, OBS LAI, $x = 0.85$, α_{leaf} PAR = 0.8, α_{leaf} NIR = 0.2, forest floor reflectance = 0.10, $VCMAX25\_0 = 25 \times 10^{-6}$ mol m^{-2} s^{-1}, $kn = 0.17$, $Tlow = 13$°C, $Tup = 45$°C, leaf scattering coefficient 0.17, quantum yield $\varepsilon = 0.06$ (mol CO2[mol PAR photons]$^{-1}$), Jarvis $Rstmin = 100$ s m^{-1}, silty clay loam with $wsat = 0.477$, $wfc = 0.322$, $wwlt = 0.218$
2006 MeadIrrigated Rotation/ US-Ne2	Soybean C3,location (−96.4701,41.1649), elevation 362m, Nebraska [*Verma et al*. 2005]	Canopy height varies with OBS LAI, $x = 0.81$, α_{leaf} PAR = 0.8, α_{leaf} NIR = 0.2, forest floor reflectance = 0.10, $VCMAX25\_0 = 90 \times 10^{-6}$ mol m^{-2} s^{-1}, $kn = 0.17$, $Tlow = 0$°C, $Tup = 36$°C, leaf scattering coefficient 0.15, quantumyield $\varepsilon = 0.08$ (mol CO2[mol PAR photons]$^{-1}$), Jarvis $Rstmin = 70$ s m^{-1}, silty clay loam with $wsat = 0.477$, $wfc = 0.322$, $wwlt = 0.218$
	U.S. EPA Measurements	
2013 DukeForest OpenField/ US-Dk1	Grasslands C3,location (−79.0934,35.9712), elevation 168m, North Carolina (*Almand-Hunter et al*. [2015])	Canopy height = 1 m, LAI = 3, $x = 0.85$, α_{leaf} PAR = 0.8, α_{leaf} NIR = 0.2, forest floor reflectance = 0.10, $VCMAX25\_0 = 26 \times 10^{-6}$ mol m^{-2} s^{-1}, $kn = 0.17$, $Tlow = 0$°C, $Tup = 36$°C, leaf scattering coefficient 0.15, quantumyield $\varepsilon = 0.12$ (mol CO2 [mol PAR photons]$^{-1}$), Jarvis $Rstmin = 100$ s m^{-1}, loam with $wsat = 0.451$, $wfc = 0.24$, $wwlt = 0.155$

capacity and is severely limited below the wilting point. Since the assimilation rate computation in the PX PSN follows the components from JULES and methods used by *Song et al*. [2009], Figure 4 compares median diurnal LH estimates from the PX PSN as well as the CO_2 assimilation parameterization methods used by JULES [*Clark et al*., 2011] and *Song et al*. [2009] (implemented in the box model) in order to make sure that the PX PSN parameterization is reasonable. The LH estimations from the different photosynthesis parameterizations are evaluated against the results from the PX Jarvis and the US-Ha1 site measurements [*Urbanski et al*., 2007] for July 2006. Although all models perform well in comparison with the observations (black line), the JULES approach tends to overestimate LH around peak photosynthesis hours because the model does not have constraints on the absorbed PAR in estimating the rate of electron transport. LH estimated using the Song approach is slightly larger than PX PSN estimations because some photosynthesis constants used by *Song et al*. [2009] are slightly different from values defined in JULES. The PX PSN, which uses the JULES approach to compute A_c, A_e and the Song's approach to compute A_j with all constants from JULES, results in better LH estimation during the peak transpiration hours. The PX Jarvis does well except in the morning hours and late evening with relatively high LH estimation. All models tend to overestimate LH during the morning and late afternoon with the photosynthesis approaches performing better in the morning. LH from the PX PSN is closest to the observations in the morning, while all photosynthesis approaches perform the best around hour 18 (6 pm). The much improved LH estimation around hour 18 has important implications for meteorology and air

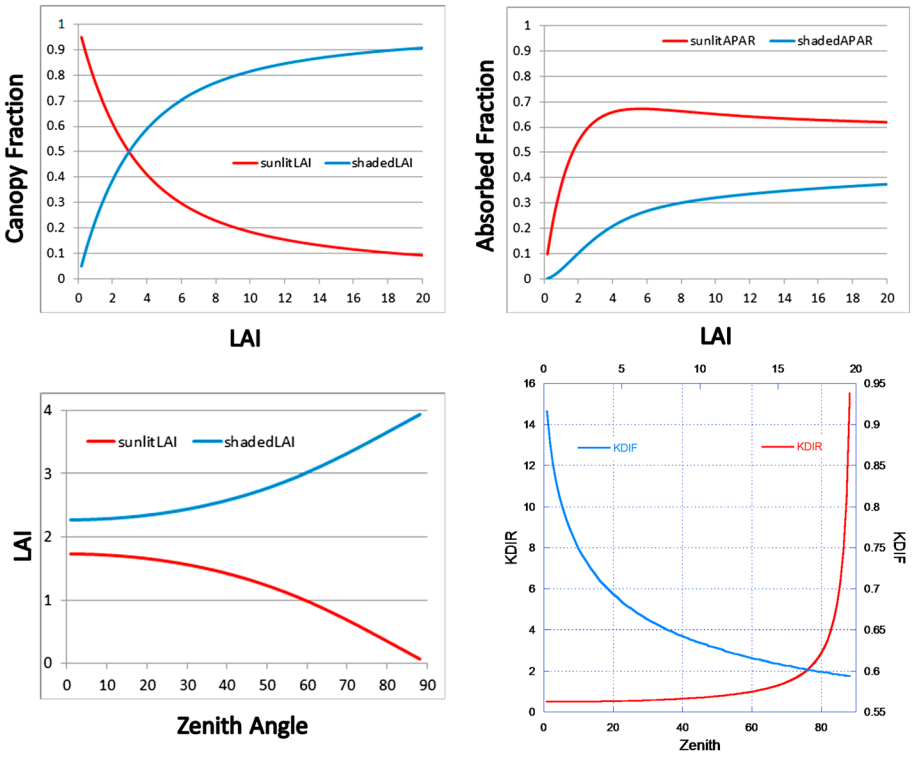

Figure 2. Canopy scaling and radiative transfer parameter plots. (top row) The leaf canopy fraction (top left) and the ratio of absorbed PAR to incident PAR (top right) for the sunlit and shaded leaves. (bottom row) The sunlit and shaded LAI (bottom left) with changing zenith angle, and the direct and diffuse extinction coefficients (bottom right) as a function of zenith angle and LAI. Parameters are computed based on US-Ha1 data on 13 June 2006 at 12 P.M. with LAI = 4 (m^2 m^{-2}) and zenith angle = 20°.

quality modeling as WRF/CMAQ tends to overestimate LH and pollutant concentrations during the evening transition when the modeled PBL tends to stabilize too quickly. Lesser LH estimation may help increase sensible heat flux, preventing premature stabilization at the surface, and thus reducing pollutant concentrations.

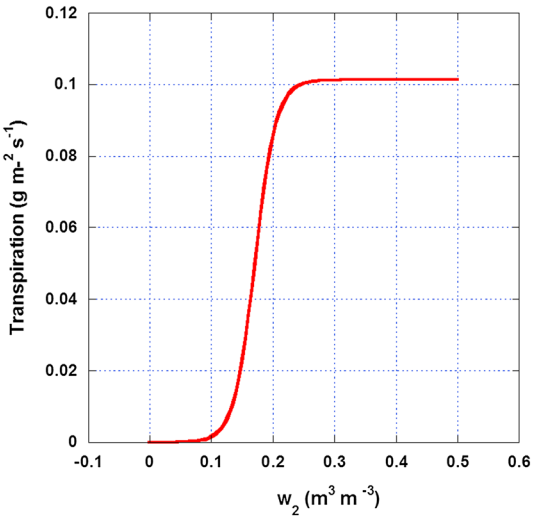

Figure 3. Transpiration as a function of deep soil moisture (w_2). Computations are based on US-Ha1 data on 2 July 2006 at 12 P.M. for loam soil.

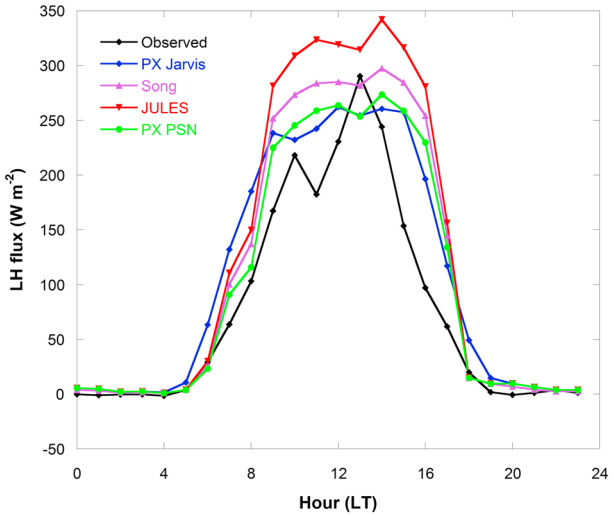

Figure 4. Diurnal median comparisons of the estimated LH from the PX PSN and the parameterization approaches used by JULES [*Clark et al.*, 2011] and *Song et al.* [2009] to compute three potential assimilation rates (A_c, A_j, and A_e) with LH from the PX Jarvis and observations at the US-Ha1 site. The FLUXNET observed LAI for the C_3 vegetation is used.

Figure 5 illustrates the response of ozone deposition velocity estimates to canopy stomatal conductance estimates from the PX Jarvis and PSN approaches over the 2 to 11 July 2006 period (chosen as an example of summer conditions for a short period without any missing data). The PX Jarvis tends to have higher stomatal conductance during this period, which results in slightly higher ozone deposition velocity. Since the ozone deposition involves several pathways including deposition to wet/dry cuticle surfaces, to soil surface, and via stomata including effects of mesophyll resistance (equations (10) and (11)), ozone deposition velocity is not simply linearly related to stomatal conductance as demonstrated by the comparison plots in Figure 5.

3.2. Additional FLUXNET Site Evaluation

3.2.1. Missouri Ozark/US-Moz Site

Figure 6 compares the simulated LH from the PX PSN at the Missouri Ozark/US-Moz FLUXNET site [*Gu et al.*, 2006] to the LH simulated from the PX Jarvis and observations. The measured LAI is much lower than the MODIS LAI for this deciduous broadleaf land cover type in the CMAQ 12 km grid cell in which the site is located. However, the peak green of MODIS LAI (phenology) parallels the measured LAI (Figure 6, middle). Using the observed LAI, the PX PSN and Jarvis approaches perform reasonably well in general (Figure 6, left) for simulations from 9 July (day 190) to 14 November (day 318) 2006. The PX PSN, however, tends to overestimate LH for most of the hours after 9 A.M. until the evening. Using the MODIS LAI, both models overestimate LH (Figure 6, right) due to higher LAI from MODIS. Scatterplots of estimated daily total LH

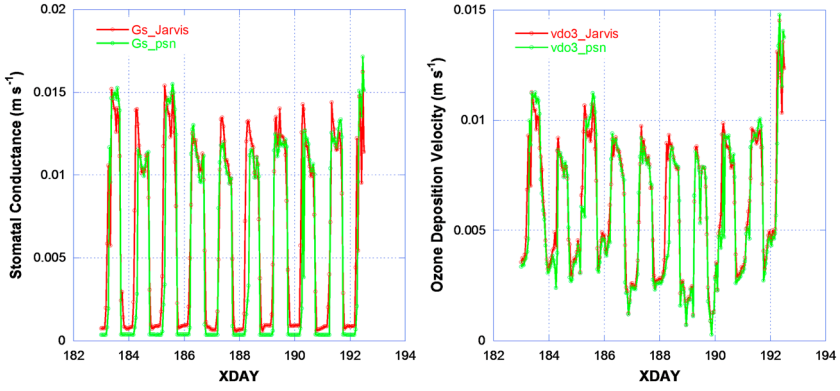

Figure 5. (left) Stomatal conductance (m s^{-1}) and (right) ozone deposition velocity (m s^{-1}) computed from the PX Jarvis and PSN approaches from 2 to 11 July 2006 at the US-Ha1 site.

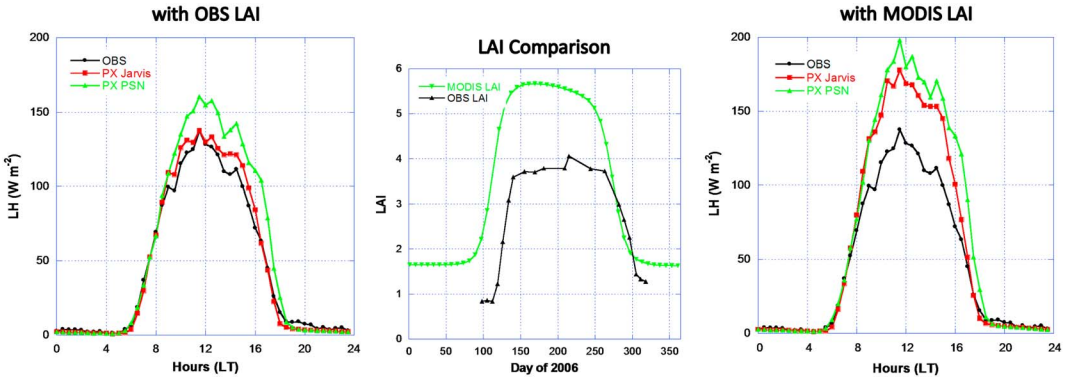

Figure 6. Missouri Ozark/US-Moz site LH diurnal median comparisons. (left) LH is simulated using the observed LAI and the (right) MODIS LAI from 9 July (190) to 14 November (318) 2006. (middle) The FLUXNET observed LAI for the C_3 vegetation and MODIS LAI for the deciduous broadleaf. Soil moisture measurements at 100 cm deep are used.

estimations against the observations (Figure 7) show that the PX Jarvis performs slightly better than the PX PSN. Ideally, the fitted regression line in the scatterplot should have a slope = 1, y intercept = 0, and $R = 1$. While the R value is quite high indicating good correlation with the observations, the slope > 1 shows a general tendency to overestimate LH by both approaches.

In contrast to the pattern at the US-Ha1 site with the same PFT (deciduous broadleaf), here the PX PSN tends to overestimate LH from midmorning to evening at the US-Moz site over the much longer simulation period (July to November versus 1 month for the US-Ha1 site). Though both sites have the same vegetation PFT, the species are different. Red oak, red maple, mature hemlock, and white pine are dominant at the US-Ha1 site, while the US-Moz site is in an oak-hickory forest which is uniquely located in an important transitional zone between hardwood and grassland in the central states. Thus, the model, which classifies both sites in the same PFT and therefore the same V_{cmax}, plant absorptivity, and other parameters, is unable to differentiate varying physiology from different trees within the same PFT at the two sites. In addition, soil moisture plays a key role in controlling the performance for the US-Moz site which has two soil moisture measurements, at 10 cm and 100 cm, in the standardized L2 data set. The soil moisture at 100 cm is almost above the field capacity for most of the year, while the soil moisture at 10 cm varies rapidly. For the first half year with almost constant deep soil moisture above the field capacity, both approaches overestimate LH significantly. During the growing season after early July, the deep soil moisture shows more variation allowing the model to be more responsive to soil moisture conditions. Thus, the simulation is conducted and analyzed over the period after

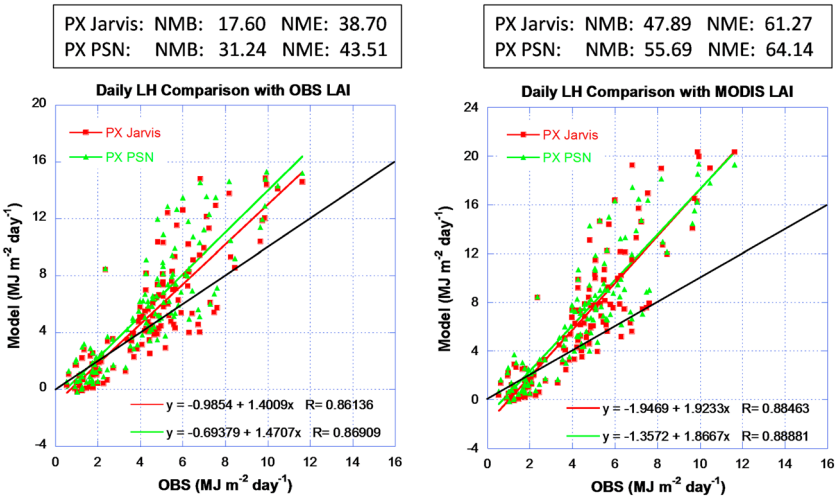

Figure 7. Missouri Ozark/US-Moz site scatterplot comparisons of daily total LH estimations. The black line is the 1:1 reference line. Days with less than 12 h of valid measurements are excluded.

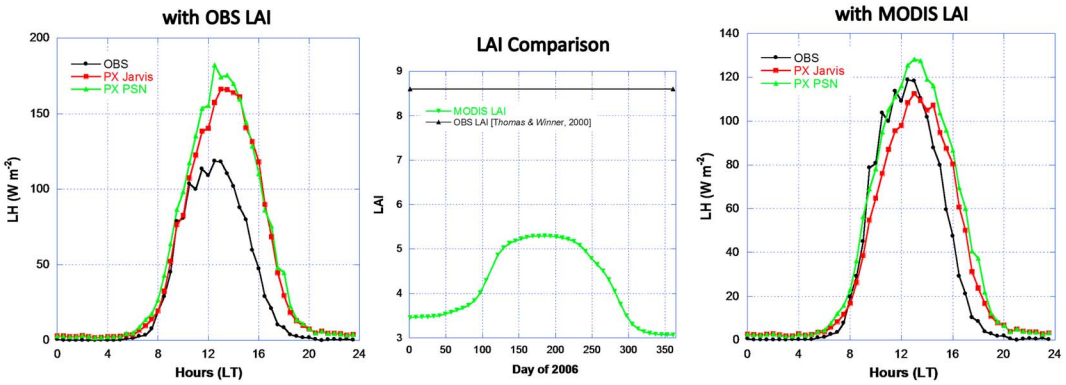

Figure 8. Wind River Field Station/US-Wrc site LH diurnal medium comparisons. LH is simulated using the (left) observed LAI and the (right) MODIS LAI from 7 January (7) to 28 November (333) 2008. (middle) The observed LAI for the C_3 vegetation [*Thomas and Winner*, 2000] and MODIS LAI for the evergreen needleleaf. Soil moisture measurements at 40 cm deep are used.

early July for this site. Through testing with soil moisture data at different depths for some of the selected sites, both models seem to perform best when using the soil moisture measured at root zone depth which is generally from 25 cm to 60 cm deep depending on the region and vegetation type (such as much deeper rooted trees in western drylands). Thus, it is crucial to choose the right soil moisture and temperature measurement for the diagnostic simulation because the measurement depths are usually different in the standardized L2 files for each FLUXNET site. Although both models use the same soil moisture limiting function F_2, the PX PSN tends to overestimate LH when soil moisture is not limiting, while the Jarvis approach generally performs better. Furthermore, it is possible that the aerodynamic surface temperature, which is calculated from observed sensible heat and used by the PX Jarvis computation, helps minimize the error in LH estimation for the tall canopy.

3.2.2. Wind River Field Station/US-Wrc Site

Simulation of LH at the Wind River Field Station/US-Wrc site is particularly challenging using the two stomatal conductance approaches in the box model. The old growth forest site is dominated by tall Douglas-fir (more than 60 m tall) more than 500 years old and tall western hemlock (more than 50 m tall). Using the observed LAI 8.6 ($m^2\,m^{-2}$) at the site [*Thomas and Winner*, 2000], both approaches significantly overestimate LH by more than 50 $W\,m^{-2}$ (Figure 8, left) for simulations from 7 January (day 7) to 28 November (day 333) 2008. Using 2006 MODIS LAI for the evergreen needleleaf land cover type reduces the overestimation of LH significantly (Figure 8, right) because the MODIS LAI (maximum around 5.3 $m^2\,m^{-2}$) is much less than the observed LAI at the site. The MODIS LAI and FPAR algorithms tend to be saturated at high LAI [*Yang et al.*, 2006]. The PX PSN has higher estimation of LH than the PX Jarvis in general for this site. With MODIS LAI, the PX PSN slightly overestimates LH while the PX Jarvis slightly underestimates around the peak radiation hour. From the late afternoon, both the approaches overestimate LH. The scatterplot evaluation is not conducted for this site due to the poor performance from both approaches over the long simulation period. The 2008 FLUXNET measurement data are used for the modeling because the 2006 measurements have too many gaps and most of the soil moisture data are missing. Since FLUXNET does not have the biological data with measured LAI for this site, the observed LAI [*Thomas and Winner*, 2000] over late 1990s and available 2006 MODIS LAI for WRF/CMAQ are used for the simulation with the assumption that LAI does not change too much for this old growth site PFT. The MODIS LAI does show seasonal variation which peaks in late spring for the vegetation in this area with wet cool winters and hot dry summers.

Similar to other sites, the model seems to be very sensitive to the soil moisture data at the Wind River site. Soil moisture measurements are available at eight different depths between 0 to 2 m for this site (not in the standardized L2 data). The measurement at 40 cm which shows most reasonable variations during the hot summer is selected for modeling. However, the soil moisture is mostly above the field capacity during the rest of the year which results in LH overestimation for the first of the half year (similar to the situation at the US-Moz site). With most plant roots within 0.5 m, deep roots extending to 1–2 m deep and fine roots in the top 0–0.3 m deep [*Shaw et al.*, 2004], it seems that the soil moisture measurements used for the modeling are

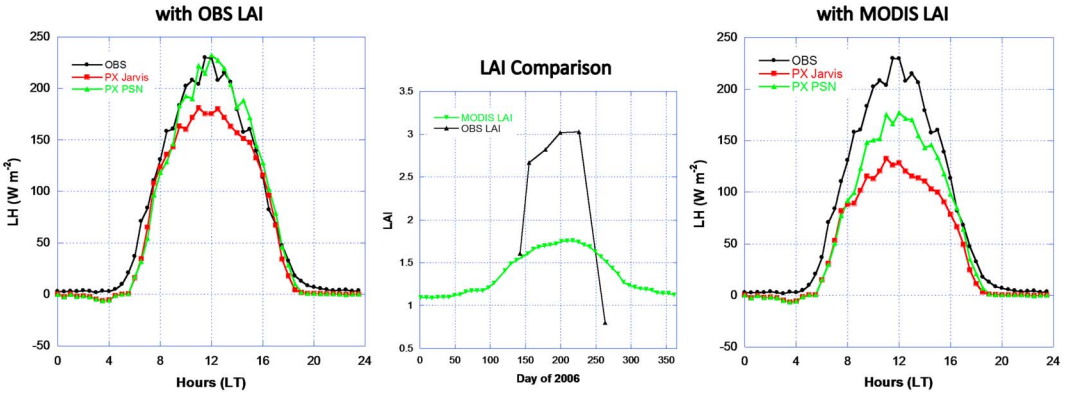

Figure 9. Fermi Prairie/US-IB2 site LH diurnal median comparisons. LH is simulated using the (left) observed LAI and the (right) MODIS LAI from 22 May (142) to 20 September (263) 2006. (middle) The FLUXNET observed LAI for the C_4 grassland and MODIS LAI for the grassland. Soil moisture measurements at 25 cm deep are used.

too deep for the cool seasons but about right for the dry seasons. This indicates that the optimal soil moisture depth for modeling plant transpiration not only varies with different sites and vegetation composition but also with different seasons depending on the soil moisture demand by vegetation. This may be particularly important for the US-Wrc site which has diverse vegetation species composition and canopy structures. Furthermore, the more than 500 year old tall Douglas-fir and western hemlock that are dominant at the site present ecological modeling complexity regarding age, height, biomass, and understory/overstory structures. Many studies [*McDowell et al*., 2002; *Phillips et al*., 2002; *Wharton et al*., 2009; *Pangle et al*., 2015] have investigated the relationship between the canopy flux of water and tree height since *Ryan and Yoder* [1997] first proposed the hydraulic limitation hypothesis. With the increased path from soil to the canopy stoma for tall trees, it is assumed that leaf-specific hydraulic conductance may decrease resulting in reduced stomatal conductance. *McDowell et al*. [2002] and *Phillips et al*. [2002] tested the hypothesis at the US-Wrc site with young and old Douglas-fir trees, and their results do not support the hypothesis as there is no observed decrease of stomatal conductance and photosynthesis for the old growth trees compared to the younger shorter trees from their summer observations. They suggest that old tall Douglas-fir trees may evolve to compensate for the hydraulic limitation by having more efficient sap conductance. The study by *Pangle et al*. [2015] shows that the hydraulic limitation hypothesis is supported by all species they measured including western hemlock except Douglas-fir in the Pacific Northwest. Also, since FLUXNET measurements are based on the eddy covariance method to directly measure the flux density above the canopy, the direct measurement method comes with the assumption that the terrain is flat and with uniform vegetation and that the atmosphere is in steady state. Thus, eddy covariance derived fluxes include significant uncertainties due to nonideal conditions in natural, heterogeneous landscapes, which is particularly true for this site with measurement height at 85 m above the ground over the tops of the clumped conifer canopy with diverse understory species. Accuracy of turbulent fluxes from this method is around 5–15% for the sensible heat and 10–20% for latent heat [*Mauder et al*., 2006; *Foken*, 2008] with systematic errors from sensor configurations and turbulence data processing around 5–10% and random errors from natural variation in vegetation and atmospheric turbulence around 5% [*Baldocchi*, 2008]. Since only the flux from the small eddies is measured at almost all FLUXNET network sites, some portion of the flux from larger eddies and advection is missing [*Finnigan et al*., 2003]. Larger eddies may play a role because of the 85 m measurement height at the site. Finally, turbulent flux computation in LSMs uses empirically determined nondimensional profile functions in accordance with MOST even though MOST is defined under ideal environments. The validity of MOST is limited to flat terrain with homogeneous landscape and land cover and to a steady and horizontally homogeneous flow by averaging from 10 min to around an hour [*Monin and Obukhov*, 1954]. Even under ideal environments, MOST has around 10–20% errors [*Foken*, 2006]. In nonideal conditions, MOST-based model calculations will be less accurate and result in more uncertainties in estimating aerodynamic resistance [*Wang and Dickinson*, 2012]. Given the uncertainty associated with flux measurement and computation for both model estimates and observations across the sites, caution should be used when interpreting model performance differences.

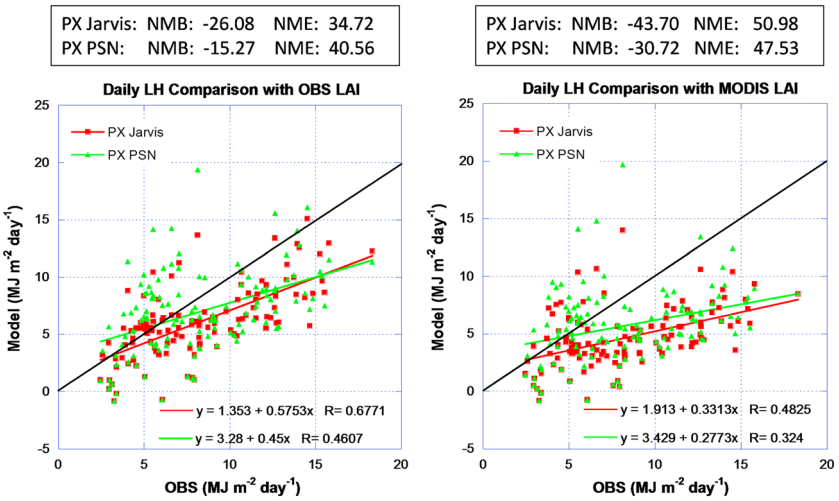

Figure 10. Fermi Prairie/US-IB2 site scatterplot comparisons of daily total LH estimations. Plot descriptions are the same as those in Figure 7.

3.2.3. Fermi Prairie/US-IB2 Site

The performance of simulated LH from 22 May (day 142) to 20 September (day 263) 2006 for the C_4 tall grass prairie at the Fermi Prairie/US-IB2 site is evaluated and shown in Figure 9. Soil moisture measurements at 25 cm deep (not in the standardized L2 data) are used for the modeling. Using the observed LAI, the PX PSN performs well while the PX Jarvis underestimates LH by about 50 ($W\,m^{-2}$) around peak radiation hours. Both approaches tend to underestimate LH in early morning and evening hours. The PX PSN treats C_3 and C_4 plants differently when modeling CO_2 assimilation, which then seems to give it an advantage when modeling LH for C_4 species in high light, dry, and hot environments. The peak MODIS LAI (around 1.75 $m^2\,m^{-2}$) is much lower than the observed LAI (around 3 $m^2\,m^{-2}$; Figure 9, middle). But, the MODIS LAI peaks coincide with the observed LAI peak in late July and early August. In general, the MODIS LAI cannot capture the peak and low LAI values compared to site observations (exception at the US-Moz site) due to averaging at the WRF/CMAQ 12 km modeling resolution. With MODIS LAI, both the approaches underestimate LH, with the PX PSN by about 50 ($W\,m^{-2}$) and the PX Jarvis by about 100 ($W\,m^{-2}$) around noon (Figure 9, right). Both approaches have high uncertainties in the daily total LH estimations as indicated by the relatively low *R* value (Figure 10). The PX PSN has lower NMB and higher NME for daily total LH estimations than the PX Jarvis for simulations with observed LAI. For MODIS LAI simulations, the PX PSN performs better with lower NMB and NME. Since this tall grassland site has rather uniform landscape with homogeneous vegetation and flat terrain [*Allison et al*., 2005], it meets the assumptions of the eddy covariance FLUXNET measurement and the turbulent flux computation by MOST relatively well in comparison with the previous two FLUXNET sites located in landscape transitional zones. Thus, both measurements and flux computations are likely to be less error prone, and the demonstrated diurnal strength of the PX PSN approach is likely to be robust.

3.2.4. Mead Irrigated Rotation/US-Ne2 Site

The box model is further evaluated for soybean crop at the Mead Irrigated Rotation/US-Ne2 site [*Verma et al*., 2005] from 12 June (day 163) to 5 October (day 278) 2006. Soil moisture is set to field capacity due to irrigation. Distinct from the other sites with constant plant height, the measured, seasonally varying crop height along with LAI from the site biological data set is used in the simulation. While both models perform well with the observed LAI and crop height (Figure 11, left), in the early morning the two models tend to underestimate LH. The PX PSN tends to overestimate LH in the early afternoon, while the PX Jarvis slightly underestimates. The PX Jarvis LSM was originally developed based on soybean measurements in Kentucky [*Pleim et al*., 2001]; thus, it is not surprising that it performs well at this site for soybeans. The fact that the PX PSN performs as well as the PX Jarvis for this crop validates its potential applicability for modeling agricultural crop land category in PX LSM. The peak LAI for soybeans can reach 5 ($m^2\,m^{-2}$) with canopy height around 1 m, but the peak MODIS LAI is only around 2.75 ($m^2\,m^{-2}$). The height of the plant follows the LAI until the leaves senesce (greenness or LAI declining to zero) just before harvesting. The soybeans were planted on 1 May (day 121) and harvested on 5 October (day 278) for 2006. According to the measurements, it took almost a month after

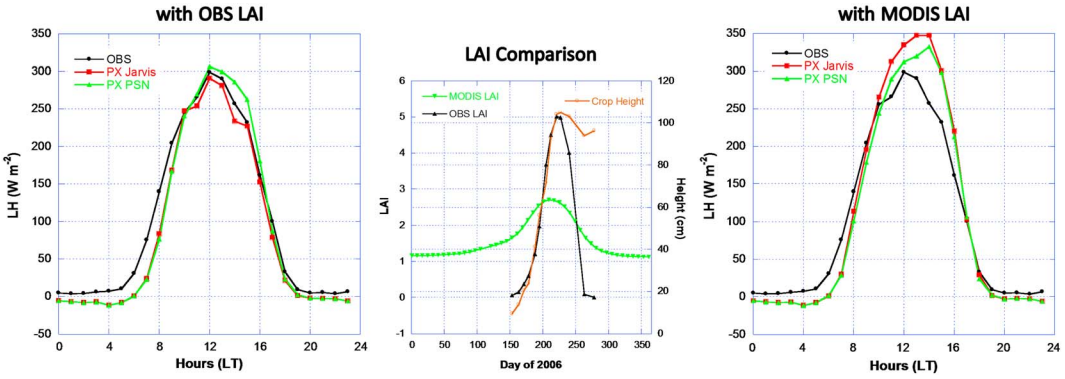

Figure 11. Mead Irrigated Rotation/US-Ne2 site LH diurnal median comparisons. LH is simulated using the (left) observed LAI and the (right) MODIS LAI from 12 June (163) to 5 October (278) 2006. (middle) The FLUXNET observed LAI and crop height for the C_3 soybean and MODIS LAI for the cropland. Soil moisture is set to field capacity.

planting for the plants to have measurable LAI. Similar to other sites, the MODIS LAI peaks coincident with the observations but cannot capture the high and low of the observed LAI at the site. With MODIS LAI, both models overestimate LH because the peak soybean LAI period is short and on average MODIS LAI is higher than the observations over the modeling period. Using the MODIS LAI, the estimated LH median from the PX PSN is close to observations around noon while the PX Jarvis overestimates LH by about 50 ($W\,m^{-2}$) and both models tend to underestimate LH in the early morning hours. The two approaches perform well in daily total LH estimations with lower NMB and NME from the PX Jarvis (Figure 12, left) in simulations with the observed LAI. Neither approach, however, performs well with the MODIS LAI which results in much higher errors and scatter (much lower R values), in spite of smaller bias (Figure 12, right). Thus, accurate LAI as well as crop height is crucial for simulations over crop lands. Because crop lands are treated as one land cover category in the current WRF/CMAQ system, the mesoscale model cannot distinguish LAI and crop height associated with planting, fertilizing, irrigating, and harvesting of different crops. Although MODIS LAI tends to be low for the peak growing season at this soybean site, it does provide some seasonalities which are related to natural (e.g., temperature and precipitation) and human influences in comparison with the table-prescribed landscape in the current system.

3.3. Ozone Site Evaluation

Simulated LH, stomatal conductance, and ozone deposition and flux from the PX Jarvis and PSN approaches over 40 days from 17 May to 18 June and 18 to 28 September 2013 are evaluated against the flux

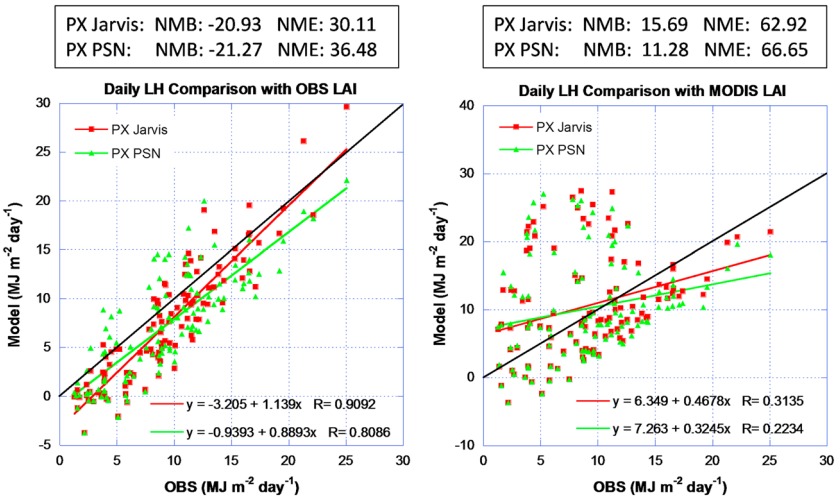

Figure 12. Mead Irrigated Rotation/US-Ne2 site scatterplot comparisons of daily total LH estimations. Plot descriptions are the same as those in Figure 7.

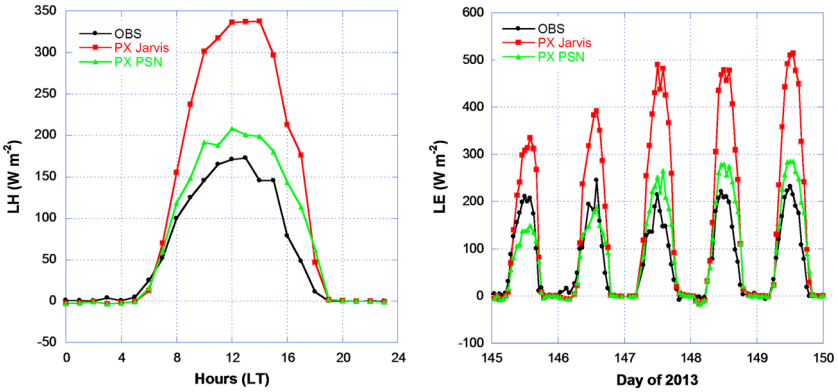

Figure 13. Duke Forest Open Field/US-Dk1 site (left) LH diurnal median and (right) selected hourly comparisons. Simulations are conducted based on LAI = 3 ($m^2\ m^{-2}$) for the C_3 grassland (tall fescue) for the periods of 17 May (day 137) to 18 June (day 169) and 18 to 28 September (days 261 to 271) 2013 with measurements. Hourly display is for 25 to 30 May 2013 (days 145 to 150).

measurements conducted by U.S. EPA at the Duke Forest Open Field/US-Dk1 site [*Almand-Hunter et al.*, 2015]. Soil temperature and volumetric water content used are the average measurements over 0–5 cm depth used in site measurement data processing. Figure 13 shows the diurnal median statistics (left) and selected 5 day hourly estimations (right) of LH using the two models against the observations. The PX Jarvis significantly overestimates LH by a factor of about 2 (~170 $W\ m^{-2}$), while the PSN overestimates LH by about 50 $W\ m^{-2}$. The hourly estimation plot for the selected 5 days shows a similar pattern with significant overestimation from PX Jarvis, while the PX PSN underestimates LH for the first 2 days (days 145 and 146) and overestimates LH for the last 3 days. The stomatal conductance estimated from the PX Jarvis is much greater than that from the PX PSN (by about a factor of 2; Figure 14, left). Similarly, ozone deposition velocity and computed ozone flux based on ozone concentration measurements are also higher from the PX Jarvis but by a smaller margin because of influences of other ozone deposition pathways. The peak ozone deposition velocity from the PX PSN is lower than the observation peak, but the peak timing follows the observations well in the early morning (Figure 14, middle). The estimated ozone flux diurnal distribution from the PX PSN (Figure 14, right) matches the observations much better than the estimations from the PX Jarvis. However, estimated ozone deposition velocity and flux are high in both models from the afternoon to late evening with the PX PSN overestimating to a much lesser degree. The daily total LH and O_3 flux estimations both show better agreement with the observation from the PX PSN with much lower NMB and NME (Figure 15). While the scatterplots show good correlations for both LH and O_3 fluxes (R values > 0.7), a factor of 2 overprediction by the PX Jarvis for LH is reflected in the slope of the regression line (slope > 2). The overprediction of O_3 flux by the PX Jarvis is evident from the scatterplot with all but 4 points above the 1-to-1 line. The low slope of the regression line and high y intercept for the PX PSN indicates a tendency to overpredict at the low end and underpredict at the high end.

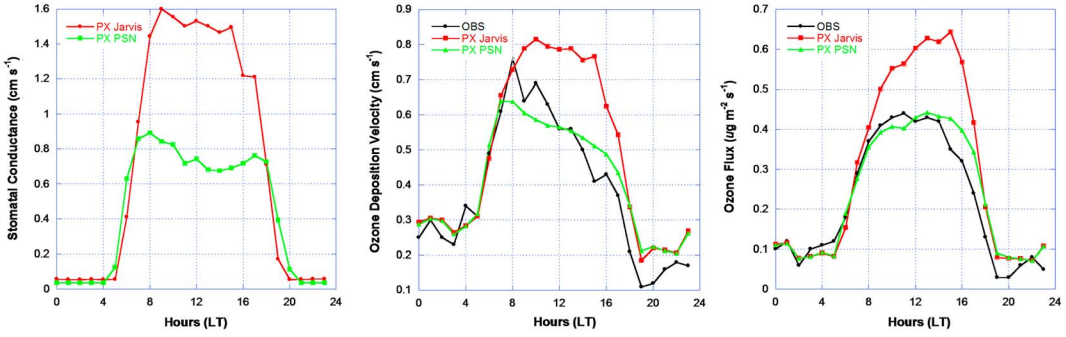

Figure 14. Duke Forest Open Field/US-Dk1 site diurnal median comparisons for (left) estimated stomatal conductance ($cm\ s^{-1}$), (middle) ozone deposition velocity ($cm\ s^{-1}$), and (right) ozone flux ($\mu g\ m^{-2}\ s^{-1}$).

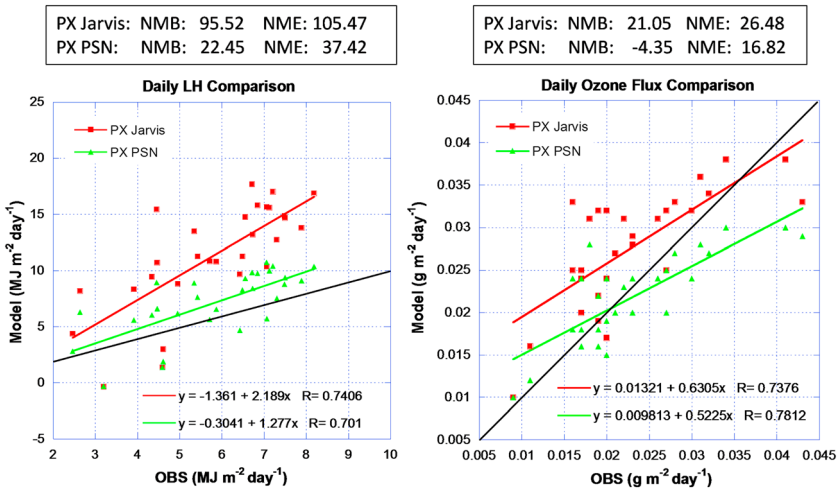

Figure 15. Duke Forest Open Field/US-Dk1 site scatterplot comparisons of daily total LH and ozone flux estimations. Plot descriptions are the same as those in Figure 7.

The big difference between the PX Jarvis and PSN approaches at this site seems to be much larger than the differences demonstrated by the four FLUXNET site evaluations discussed above. The use of measured sensible heat flux by the PX Jarvis for computing the aerodynamic surface temperature to be used in stomatal conductance computation as the leaf surface temperature may be degrading the model performance at this site. This approach seems to benefit the PX Jarvis at the Missouri Ozark/US-Moz and Wind River Field Station/US-Wrc sites which have tall tree canopies that serve as a barrier between the ground and the atmosphere. Since the surface energy budget is dominated by the canopy at these forest sites, the aerodynamic surface temperature is a good surrogate for leaf temperature. At the Duke site, the computed aerodynamic surface temperature is much higher than the ambient temperature around the noon hours (e.g., around 6° C) because the surface energy is more influenced by the ground rather than the grasses which have much less mass and volume than forest. Thus, the aerodynamic surface temperature is not as good of a surrogate for the leaf temperature. The higher leaf temperature results in a higher mixing ratio gradient between the leaf stomata and the ambient atmosphere which drives greater LH flux. In the full PX LSM with WRF/CMAQ, the difference between the two approaches are likely to be much smaller because there is full energy budget with sophistical radiation models and dynamic feedbacks which will be equally applied to both approaches at a time scale of less than 40 s.

4. Conclusions and Future Work

A coupled photosynthesis and stomatal conductance approach with simple parameterization is implemented and evaluated in a diagnostic box model with ET and ozone deposition components from WRF/CMAQ with the PX LSM. The performance of the diagnostic model is influenced by many factors including parametrizations based on broad PFTs, site-related input data, and measurement errors in addition to physical process formulations. Results from the box model comparisons should be interpreted with caution because offline simulations cannot completely represent the performance in the full-scale model with real-time feedbacks [*Qu and Henderson-Sellers*, 1998; *Samuelsson et al*., 2003]. The purpose for this study is not to develop a site-specific model which matches measurements, but rather to develop applicable algorithms to be applied to the mesoscale WRF/CMAQ simulations for realistic treatments of grid cell average surface fluxes of heat, moisture, and trace chemical species. The performance of the implemented model over varieties of vegetation and landscape types at the selected sites demonstrates that the model is applicable in large-scale modeling with diverse environments (i.e., deciduous and coniferous forest, grassland, and cropland).

The photosynthesis-based approach is constrained by many additional model parameters, particularly related to photosynthesis such as the maximum rate of carboxylation of Rubisco-V_{cmax}, the foliage nitrogen decay coefficient-K_n, maximum electron transport rate-J_{max}, and quantum yield-ε. This gives the model advantages in distinguishing plants with different photosynthesis mechanism (C_3 and C_4) and efficiency

among PFTs (such evergreen or deciduous from boreal, temperate, or tropic regions, different crops). However, those parameter values vary among and within PFTs across literature and different models. It is important to choose the values which represent plant types for the modeling approach including scaling implemented in the full Eulerian grid model. The model performs differently even at the sites with same PFT (such as US-Ha1 and US-Moz sites with broadleaf deciduous trees) using the same photosynthesis-related parameters due to different vegetation composition. In addition, LAI and soil moisture and texture influence the performance of the both approaches.

The evaluation using observed LAI and MODIS LAI processed for the WRF/CMAQ 12 km grid domain shows that accurate LAI is important for matching site measurements. With the MODIS LAI input, both approaches perform worse, relative to observed LAI, except at the Wind River Field Station US-Wrc site where lower LAI from averaged MODIS LAI at WRF/CMAQ grid cells helps reduce LH and matches the observations well. Although the MODIS LAI is generally different from the observed LAI, the change of MODIS LAI over the growing season does peak with the observed LAI. Thus, MODIS LAI captures the seasonality (or phenology) of vegetation, that is consistent with the results from *Ran et al*. [2015, 2016]. Note that, in the full Eulerian grid model, LSM performance is improved through real-time soil moisture and temperature nudging in the WRF PX LSM [*Pleim and Xiu*, 2003; *Pleim and Gilliam*, 2009] which continually adjusts soil moisture and temperature to reduce errors in LH flux thereby reducing air temperature and humidity errors. This scheme compensates for model errors due to inaccurate parameters as well as oversimplified canopy and soil algorithms. Thus, even though the box model simulations use whatever soil moisture measurements that are available, the overestimation of LH which is observed at most sites is likely to be corrected in WRF simulations with the PX LSM soil nudging scheme and dynamic feedbacks.

The photosynthesis-based approach is evaluated at the Harvard Forest (US-Ha1) FLUXNET site for July 2006, and the model performs well in comparison with the PX Jarvis approach and two other CO_2 assimilation methods compared to observations. The PX PSN can simulate LH as well as the PX Jarvis in general for four selected FLUXNET sites (US-Moz, US-Wrc, US-IB2, and US-Ne2), though the performance varies at different sites. For the US-Moz and US-Wrc sites with tall forest canopy, the PX Jarvis approach shows some advantages during the peak noon hours. The PX PSN shows clear improvement in modeling short vegetation (e.g., grassland and soybean), particularly for the C_4 grassland at the Fermi Prairie US-IB2 site by distinguishing C_3 and C_4 plants in modeling the CO_2 assimilation rate. Both the approaches significantly overestimate LH at the Wind River Field Station US-Wrc site with observed LAI because of the complex landscape dominated by old growth tall Douglas-fir and western hemlock. As the PX PSN is a single-layer two-leaf model for mesoscale modeling, it shows limitation in modeling sites with complex canopy structures including different species at different heights. For the complex canopy, a multilayer model [*Baldocchi and Meyers*, 1998; *Meyers et al*., 1998] likely performs better. The advanced model performs much better than the PX Jarvis at the Duke Forest Open Field US-Dk1 grassland site in simulating LH and ozone flux. The PX PSN shows the ability to simulate the diurnal shape of ozone deposition velocity which usually peaks in the early morning. The Jarvis approach is known to have difficulty in simulating the diurnal shape [*Finkelstein et al*., 2000; *Pleim et al*., 2001], and this deficiency is clearly demonstrated at the site. The simulated ozone flux from the advanced approach matches the observations much better than that from the PX Jarvis which overestimates ozone flux by about 50%.

The current PX WRF/CMAQ uses 20-class NLCD land cover types [*Anderson et al*., 1976] for the U.S. and 20-class MODIS International Geosphere-Biosphere Programme types [*Belward*, 1996] for areas outside the U. S. [*Ran and Hanna*, 2016]. There is an ongoing effort at U.S. EPA to develop new land cover classes with detailed PFTs for vegetation from boreal, temperate, tropical, and dryland regions and with major crop categories including irrigation information. The new land cover types with more specific PFTs are more suitable for the photosynthesis-based PX LSM than the current land cover types used in the system. With realistic MODIS vegetation being ingested into WRF/CMAQ [*Ran et al*., 2016], the system has more accurate vegetation and surface representation which helps improve not only spatial and temporal characteristics of vegetation and land surface but also improves the meteorology performance. The next step is to implement the evaluated PX PSN into the system. Thus, the system with improved land surface representation and vegetation processes can be used in research and applications in coupling air quality, climate, and vegetation productivity directly with CO_2 concentration which changes temporally and spatially. In addition, the effects of air pollutants such as O_3 on ecosystem productivity can also be easily implemented in this advanced

approach [*Sitch et al*., 2007; *Lombardozzi et al*., 2012] for the U.S. EPA's secondary standard assessments under the Clean Air Act to protect the environment.

Appendix A: CO_2 Assimilation Rates

The Rubisco-limited assimilation rate (A_c mol CO_2 m^{-2} s^{-1}) is a function of the maximum rate of carboxylation of Rubisco (V_{cmax} mol CO_2 m^{-2} s^{-1}) and is formulated following equation (1) in the paper by *Clark et al*. [2011] for JULES. Following equation (4) in *Clark et al*. [2011], V_{cmax} at any leaf surface temperature is estimated based on the maximum rate of carboxylation of the enzyme Rubisco at 25°C (V_{cmax25} mol CO_2 m^{-2} s^{-1}), limited by the assumed optimal temperature range for specific plant function type (PFT). The average V_{cmax25} value is assumed to be related to leaf nitrogen concentration and is computed based on the top of the canopy V_{cmax25} (V_{cmax25_0}) integrated for sunlit and shaded leaves based on the equations described by *Bonan et al*. [2011] as

$$V_{cmax25}(\mathrm{sun}) = V_{cmax25\_0}\left(1 - e^{-(K_n+K_{\mathrm{dir}})\mathrm{LAI}}\right)\frac{1}{K_n + K_{\mathrm{dir}}}\frac{1}{\mathrm{LAI}_{\mathrm{sun}}} \tag{A1}$$

$$V_{cmax25}(\mathrm{sha}) = V_{cmax25\_0}\left\{\left(1 - e^{-K_n\mathrm{LAI}}\right)\frac{1}{K_n} - \left(1 - e^{-(K_n+K_{\mathrm{dir}})\mathrm{LAI}}\right)\frac{1}{K_n + K_{\mathrm{dr}}}\right\}\frac{1}{\mathrm{LAI}_{\mathrm{shd}}} \tag{A2}$$

where K_n is the foliage nitrogen decay coefficient, K_{dir} is the direct beam attenuation coefficient within the canopy (described by equation (B3)), and $\mathrm{LAI}_{\mathrm{sun}}$ and $\mathrm{LAI}_{\mathrm{shd}}$ are the LAI values for sunlit and shaded leaves (described by equations (B1) and (B2)). As one of the most important parameters in the photosynthesis approach, V_{cmax25} shows a range of values among and within PFTs [*Kattge et al*., 2009] mainly due to different nitrogen use efficiencies. The value used is often tightly related to the foliage nitrogen decay coefficient (K_n) which also varies among models [*Bonan et al*., 2011]. The PX LSM photosynthesis model follows the V_{cmax25} values after nitrogen constraints from *Clark et al*. [2011] and assigns $K_n = 0.17$ based on the values analyzed by *Bonan et al*. [2011]. *Bonan et al*. [2011] uses $K_n = 0.11$ in their evaluation study; but the value is set to 0.3 in CLM4.5 for multilayer model considerations [*Oleson et al*., 2013].

The light-limited assimilation rate (A_j mol CO_2 m^{-2} s^{-1}) is a function of the rate of electron transport (J mol electron m^{-2} s^{-1}) and is computed as

$$A_j = \begin{cases} J\left(\dfrac{c_i - c_c}{4.5c_i + 10.5c_c}\right) & \text{for } C_3 \text{ plants} \\ \varepsilon I_{\mathrm{apar}} & \text{for } C_4 \text{ plants} \end{cases} \tag{A3}$$

with

$$0.7J^2 - \left(\varepsilon_j I_{\mathrm{apar}} + J_{\mathrm{max}}\right)J + \varepsilon_j I_{\mathrm{apar}} J_{max} = 0 \tag{A4}$$

$$\varepsilon_j = \varepsilon\frac{4(c_i + 2c_c)}{(c_i - c_c)} \tag{A5}$$

$$J_{\mathrm{max}} = 1.97V_{cmax} \tag{A6}$$

where J is solved using the quadratic equation (A4), ε is the quantum yield (mol CO_2 [mol PAR photons]$^{-1}$), and ε_j (mol CO_2 [mol PAR photons]$^{-1}$) is the computed electron transport quantum use efficiency following the study by *Medlyn et al*. [2005] and applied in *Song et al*. [2009]. c_i (Pa) is the CO_2 partial pressure inside the leaf stomata. c_c (Pa) is the CO_2 compensation point in the absence of nonphotorespiratory respiration, which is computed following equation (7) in the paper by *Clark et al*. [2011]. J_{max} is the maximum electron transport rate (mol electron m^{-2} s^{-1}) and is estimated to be 1.97 times V_{cmax} following *Bonan et al*. [2011]. I_{apar} (PAR, mol m^{-2} s^{-1}) is the absorbed photosynthetically active radiation (APAR) by the leaf. The photosynthesis rate (A_e) limited by the transport of photosynthetic products for C_3 plants and PEP carboxylase limitation for C_4 plants is computed following equation (3) in *Clark et al*. [2011].

The final CO_2 assimilation rate (A) is computed by solving the colimitation equations as described by *Bonan et al.* [2011] shown in equations (A7) and (A8), and the net CO_2 assimilation rate is computed by subtracting leaf dark respiration from A as

$$0.98A_i^2 - (A_c + A_j)A_i + A_cA_j = 0 \tag{A7}$$

$$0.95A^2 - (A_i + A_e)A + A_iA_e = 0 \tag{A8}$$

$$A_{\text{net}} = A - f_{\text{dr}}V_{\text{cmax}} \tag{A9}$$

where A_i is the smoothed minimum of A_c and A_j. A_i and A are the smallest roots of the quadratic equations. f_{dr} is the dark respiration coefficient which is set to 0.015 for C_3 plants and 0.025 for C_4 plants following JULES.

Appendix B: Canopy Scaling and Radiative Transfer

The sunlit (LAI_{sun}) and shaded (LAI_{shd}) leaf areas are computed using the equations described by *Campbell and Norman* [1998] as

$$\text{LAI}_{\text{sun}} = \frac{1 - e^{-K_{\text{dir}}\text{LAI}}}{K_{\text{dir}}} \tag{B1}$$

$$\text{LAI}_{\text{shd}} = \text{LAI} - \text{LAI}_{\text{sun}} \tag{B2}$$

Campbell [1986] suggested a simple equation to compute the direct beam attenuation coefficient (K_{dir}) as

$$K_{\text{dir}} = \frac{\sqrt{x^2 + \tan^2(\theta_{\text{sun}})}}{x + 1.774(x + 1.182)^{-0.733}} \tag{B3}$$

where θ_{sun} is the solar zenith angle, and x is the canopy leaf orientation parameter with 0 for vertical leaves and 1 for spherical leaf orientation (randomly oriented). Following the work by *Goudriaan* [1977], the transmittance of beam radiation for nonhorizontal scattering leaves with leaf absorptivity (α_{leaf}) can be computed as

$$\tau_{\text{dir}} = e^{-\sqrt{\alpha_{\text{leaf}}}K_{\text{dir}}\text{LAI}} \tag{B4}$$

The extinction coefficient for diffuse light (K_{dif}) within the canopy can be estimated by first computing the transmittance for diffuse radiation for the upper hemisphere (τ_{dif}) as

$$\tau_{\text{dif}} = \int_0^{\pi/2} \exp(-K_{\text{dir}}(\theta_{\text{sun}})\text{LAI})\sin(2\theta_{\text{sun}})\text{d}\theta_{\text{sun}} \tag{B5}$$

$$K_{\text{dif}} = -\frac{\ln(\tau_{\text{dif}})}{\text{LAI}} \tag{B6}$$

The mean radiation intensity on the sunlit and shaded leaves from visible (or PAR) and near infrared (NIR) bands are estimated based on the direct and diffuse PAR and NIR radiation estimations at the top canopy using the methods described by *Song et al.* [2009]. The net radiation (R_{net}) for the sunlit and shaded leaves is computed individually as

$$R_{\text{net}} = \text{APAR} + \text{ANIR} + \text{LW}_{\text{floor}}f_{\text{LW}} + \text{LW}_{\text{air}}f_{\text{LW}} - 2\text{LW}_{\text{canopy}}f_{\text{LW}} \tag{B7}$$

with

$$f_{\text{LW}} = \frac{1 - \exp(-K_{\text{dif}}\text{LAI})}{K_{\text{dif}}\text{LAI}} \tag{B8}$$

where APAR and ANIR are the absorbed PAR and NIR at the leaf (sunlit or shaded) (W m^{-2}), LW_{floor}, LW_{air}, and $\text{LW}_{\text{canopy}}$ are the long wave radiations (W m^{-2}) from the floor, air, and canopy computed following the methods of *Song et al.* [2009], and f_{LW} is the scaling factor of the longwave radiation to the canopy. The leaf temperature is computed following the method described by *Evers et al.* [2010] using the Penman-Monteith equation with R_{net} computed for each leaf.

Disclaimer

While this work has been reviewed and cleared for publication by the U.S. EPA, the views expressed here are those of the authors and do not necessarily represent the official views or policies of the Agency.

Acknowledgments
MODIS LAI/FPAR data used by the paper are available at the North American Carbon Program (http://nacarbon.org/nacp/data.html). FLUXNET data used by this paper are available from AmeriFlux Site and Data Exploration System (http://ameriflux.ornl.gov/). The authors would like to acknowledge the help of Ian T. Baker from Colorado State University at Fort Collins, Colorado, USA; Yongjiu Dai from Beijing Normal University, Beijing, China; and Gordon B. Bonan from University Corporation for Atmospheric Research at Boulder, Colorado, USA on the photosynthesis approach used in climate land surface modeling through the email communications. The review from Ellen Cooter at the U.S. EPA is also greatly appreciated.

References

Allison, V. J., R. M. Miller, J. D. Jastrow, R. Matamala, and D. R. Zak (2005), Changes in soil microbial community structure in a tall grass prairie chronosequence, *Soil Sci. Soc. Am. J.*, *69*(5), 1412–1421.

Almand-Hunter, B. B., J. T. Walker, N. P. Masson, L. Hafford, and M. P. Hannigan (2015), Development and validation of inexpensive, automated, dynamic flux chambers, *Atmos. Meas. Tech.*, *8*, 267–280.

Anderson, J. R., E. E. Hardy, J. T. Roach, and R. E. Witmer (1976), *A Land Use and Land Cover Classification System for Use With Remote Sensor Data*, *Professional Paper*, vol. 964, 28 p., U.S. Geological Survey, Arlington, Va.

Appel, K. W., K. M. Foley, J. O. Bash, P. W. Pinder, R. L. Dennis, D. J. Allen, and K. A. Pickering (2011), Multi-resolution assessment of the Community Multiscale Air Quality (CMAQ) model v4.7 wet deposition estimates for 2002–2006, *Geosci. Model Dev.*, *4*, 357–371.

Baker, I. T., A. S. Denning, N. Hanan, L. Prihodko, P. L. Vidale, K. Davis, and P. Bakwin (2010), North American gross primary productivity: Regional characterization and interannual variability, *Tellus*, *62B*, 533–549.

Baldocchi, D. (2008), TURNER REVIEW No. 15, 'Breathing' of the terrestrial biosphere: Lessons learned from a global network of carbon dioxide flux measurement systems, *Aust. J. Bot.*, *56*(1), 1–26.

Baldocchi, D. D., and T. Meyers (1998), On using eco-physiological, micrometeorological and biogeochemical theory to evaluate carbon dioxide, water vapor and trace gas fluxes over vegetation: A perspective, *Agric. For. Meteorol.*, *90*(1–2), 1–25.

Ball, M. C., I. E. Woodrow, and J. A. Berry (1987), A model predicting stomatal conductance and its contribution to the control of photosynthesis under different environmental conditions, in *Progress in Photosynthesis Research*, edited by J. Biggins, pp. 221–224 , Martinus Nijhoff Publishers, Dordrecht, Netherlands.

Belward, A. S. (Ed.) (1996), The IGBP-DIS global 1 km land cover data set (DISCover)-proposal and implementation plans, IGBP-DIS Working Paper No. 13, Toulouse, France.

Bonan, G. B. (2008), *Ecological Climatology: Concepts and Applications*, Cambridge Univ. Press, New York.

Bonan, G. B., P. J. Lawrence, K. W. Oleson, S. Levis, M. Jung, M. Reichstein, D. M. Lawrence, and S. C. Swenson (2011), Improving canopy processes in the Community Land Model version 4 (CLM4) using global flux fields empirically inferred from FLUXNET data, *J. Geophys. Res.*, *116*, G02014, doi:10.1029/2010JG001593.

Budyko, M. (1974), *Climate and Life*, Academic Press, New York.

Byun, D. W., and K. L. Schere (2006), Review of the governing equations, computational algorithms, and other components of the models-3 Community Multiscale Air Quality (CMAQ) modeling system, *Appl. Mech. Rev.*, *59*, 51–77.

Campbell, G. S. (1986), Extinction coefficients for radiation in plant canopies calculated using an ellipsoidal inclination angle distribution, *Agric. For. Meteorol.*, *36*(4), 317–321.

Campbell, G. S., and J. M. Norman (1998), *An Introduction to Environmental Biophysics*, Springer Sci. & Business Media, New York.

Chen, F., and J. Dudhia (2001), Coupling an advanced land-surface/hydrology model with the Penn State/NCAR MM5 modeling system. Part I: Model implementation and sensitivity, *Mon. Weather Rev.*, *129*, 569–585.

Chen, J. M., A. Govind, O. Sonnentag, Y. Zhang, A. Barr, and B. Amiro (2006), Leaf area index measurements at Fluxnet-Canada forest sites, *Agric. For. Meteorol.*, *140*(1), 257–268.

Clark, D. B., et al. (2011), The joint UK land environment simulator (JULES), model description—Part 2: Carbon fluxes and vegetation dynamics, *Geosci. Model Dev.*, *4*(3), 701–722.

Cohan, D. S., J. W. Boylan, A. Marmur, and M. N. Khan (2007), An integrated framework for multipollutant air quality management and its application in Georgia, *Environ. Manage.*, *40*, 545–554.

Collatz, G. J., J. T. Ball, C. Grivet, and J. A. Berry (1991), Physiological and environmental regulation of stomatal conductance, photosynthesis and transpiration: A model that includes a laminar boundary layer, *Agric. For. Meteorol.*, *54*(2), 107–136.

Collatz, G. J., M. Ribas-Carbo, and J. A. Berry (1992), Coupled photosynthesis-stomatal conductance model for leaves of C4 plants, *Aust. J. Plant Physiol.*, *19*, 519–538.

Compton, J. E., J. A. Harrison, R. L. Dennis, T. L. Greaver, B. H. Hill, S. J. Jordan, H. Walker, and H. V. Campbell (2011), Ecosystem services altered by human changes in the nitrogen cycle: A new perspective for US decision making, *Ecol. Lett.*, *14*, 804–815.

Cox, P. M., C. Huntingford, and R. J. Harding (1998), A canopy conductance and photosynthesis model for use in a GCM land surface scheme, *J. Hydrol.*, *212*(1998), 79–94.

Dai, Y., R. E. Dickinson, and Y. P. Wang (2004), A two-big-leaf model for canopy temperature, photosynthesis, and stomatal conductance, *J. Clim.*, *17*, 2281–2299.

de Pury, D. G. G., and G. D. Farquhar (1997), Simple scaling of photosynthesis from leaves to canopies without the errors of big-leaf models, *Plant Cell Environ.*, *20*, 537–557.

Eder, B., D. Kang, R. Mathur, J. Pleim, S. Yu, T. Otte, and G. Pouliot (2009), A performance evaluation of the National Air Quality Forecast Capability for the summer of 2007, *Atmos. Environ.*, *43*(14), 2312–2320.

Evers, J. B., J. Vos, X. Yin, P. Romero, P. E. L. Van Der Putten, and P. C. Struik (2010), Simulation of wheat growth and development based on organ-level photosynthesis and assimilate allocation, *J. Exp. Bot.*, *61*(8), 2203–2216.

Farquhar, G. D., S. von Caemmerer, and J. A. Berry (1980), A biochemical model of photosynthetic CO_2 assimilation in leaves of C3 species, *Planta*, *149*, 78–90.

Finkelstein, P. L., T. G. Ellestad, J. F. Clarke, T. P. Meyers, D. B. Schwede, E. O. Hebert, and J. A. Neal (2000), Ozone and sulfur dioxide dry deposition to forests: Observations and model evaluation, *J. Geophys. Res.*, *105*, 15,365–15,377, doi:10.1029/2000JD900185.

Finnigan, J. J., R. Clement, Y. Malhi, R. Leuning, and H. A. Cleugh (2003), A reevaluation of long-term flux measurement techniques—Part I: Averaging and coordinate rotation, *Boundary Layer Meteorol.*, *107*, 1–48.

Foken, T. (2006), 50 years of the Monin-Obukhov similarity theory, *Boundary Layer Meteorol.*, *119*, 431–447.

Foken, T. (2008), The energy balance closure problem: An overview, *Ecol. Appl.*, *18*(6), 1351–1367.

Foley, K. M., et al. (2010), Incremental testing of the Community Multiscale Air Quality (CMAQ) modeling system version 4.7, *Geosci. Model Dev.*, *3*(1), 205–226.

Gao, F., J. Morisette, R. Wolfe, G. Ederer, J. Pedelty, E. Masuoka, R. Myneni, B. Tan, and J. Nightingale (2008), An algorithm to produce temporally and spatially continuous MODIS-LAI time series, *IEEE Geosci. Remote Sens. Lett.*, *5*(1), 60–64.

Gilliam, R. C., and J. E. Pleim (2010), Performance assessment of new land surface and planetary boundary layer physics in the WRF-ARW, *J. Appl. Meteorol. Climatol.*, *49*(4), 760–774.

Goudriaan, J. (1977), *Crop Micrometeorology: A simulation Study*, Pudoc, Center Agric. Publ. Documentation, Wageningen, Netherlands.

Gu, L., T. Meyers, S. G. Pallardy, P. J. Hanson, B. Yang, M. Heuer, K. P. Hosman, J. S. Riggs, D. Sluss, and S. D. Wullschleger (2006), Direct and indirect effects of atmospheric conditions and soil moisture on surface energy partitioning revealed by a prolonged drought at a temperate forest site, *J. Geophys. Res.*, *111*, D16102, doi:10.1029/2006JD007161.

Hogrefe, C., G. Pouliot, D. Wong, A. Torian, S. Roselle, J. Pleim, and R. Mathur (2015), Annual application and evaluation of the online coupled WRF-CMAQ system over North America under AQMEII phase 2, *Atmos. Environ.*, *115*, 683–694.

Jarvis, P. G. (1976), The interpretation of the variations in leaf water potential and stomatal conductance found in canopies in the field, *Philos. Trans. R. Soc. London, Series B*, *273*, 593–610.

Jarvis, P. G. (1995), Scaling processes and problems, *Plant Cell Environ.*, *18*(10), 1079–1089.

Jarvis, P. G., and K. G. McNaughton (1986), Stomatal control of transpiration: Scaling up from lead to region, *Adv. Ecol. Res.*, *15*, 1–49.

Kattge, J., W. Knorr, T. Raddatz, and C. Wirth (2009), Quantifying photosynthetic capacity and its relationship to leaf nitrogen content for global scale terrestrial biosphere models, *Global Change Biol.*, *15*, 976–991.

Katul, G. G., R. Oren, S. Manzoni, C. Higgins, and M. B. Parlange (2012), Evapotranspiration: A process driving mass transport and energy exchange in the soil-plant-atmosphere-climate system, *Rev. Geophys.*, *50*, doi:10.1029/2011RG000366.

Kelly, J. T., K. R. Baker, J. B. Nowak, J. G. Murphy, M. Z. Markovic, T. C. VandenBoer, R. A. Ellis, and C. Misenis (2014), Fine-scale simulation of ammonium and nitrate over the South Coast Air Basin and San Joaquin Valley of California during CalNex-2010, *J. Geophys. Res. Atmos.*, *119*, 3600–3614, doi:10.1002/2013JD021290.

Kobayashi, H., D. D. Baldocchi, Y. Ryu, Q. Chen, S. Ma, J. L. Osuna, and S. L. Ustin (2012), Modeling energy and carbon fluxes in a heterogeneous oak woodland: A three-dimensional approach, *Agric. For. Meteorol.*, *152*(2012), 83–100.

Kowalczyk, E. A., L. Stevens, R. M. Law, M. Dix, Y. P. Wang, I. N. Harman, and T. Ziehn (2013), The land surface model component of ACCESS: Description and impact on the simulated surface climatology, *Aust. Meteorol. Oceanogr. J.*, *63*(1), 65–82.

Leuning, R., F. M. Kelliher, D. G. G. Depury, and E. D. Schulze (1995), Leaf nitrogen, photosynthesis, conductance and transpiration—Scaling from leaves to canopies, *Plant Cell Environ.*, *18*(10), 1183–1200.

Lombardozzi, D., S. Levis, G. Bonan, and J. P. Sparks (2012), Predicting photosynthesis and transpiration responses to ozone: Decoupling modeled photosynthesis and stomatal conductance, *Biogeosciences*, *9*, 3113–3130, doi:10.5194/bg-9-3113-2012.

Mauder, M., C. Liebethal, M. Gockede, J.-P. Leps, F. Beyrich, and T. Foken (2006), Processing and quality control of flux data during LITFASS-2003, *Boundary Layer Meteorol.*, *121*, 67–88.

McDowell, N. G., N. Phillips, C. Lunch, B. J. Bond, and M. G. Ryan (2002), An investigation of hydraulic limitation and compensation in large, old Douglas-fir trees, *Tree Physiol.*, *22*(11), 763–774.

Medlyn, B. E., A. P. Robinson, R. Clement, and R. E. McMurtrie (2005), On the validation of models of forest CO_2 exchange using eddy covariance data: Some perils and pitfalls, *Tree Physiol.*, *25*(7), 839–857.

Meyers, T. P., P. L. Finkelstein, J. Clarke, T. G. Ellestad, and P. F. Sims (1998), A multilayer model for inferring dry deposition using standard meteorological measurements, *J. Geophys. Res.*, *103*, 22,645–22,661, doi:10.1029/98JD01564.

Monin, A. S., and A. Obukhov (1954), Basic laws of turbulent mixing in the surface layer of the atmosphere, *Contrib. Geophys. Inst. Acad. Sci., USSR*, *151*, 163–187.

Monteith, J. L. (1981), Evaporation and surface-temperature, *Q. J. R. Meteorol. Soc.*, *107*(451), 1–27.

Moorcroft, P. R. (2006), How close are we to a predictive science of the biosphere?, *Trends Ecol. Evol.*, *21*(7), 400–407.

Myneni, R., Y. Knyazikhin, and N. Shabanov (2011), Leaf area index and fraction of absorbed PAR products from Terra and Aqua MODIS Sensors: Analysis, validation, and refinement, *Land Remote Sens. Global Environ. Change*, *11*, 603–633.

Noilhan, J., and J. F. Mahfouf (1996), The ISBA land surface parameterisation scheme, *Global Planet. Change*, *13*(1), 145–159.

Noilhan, J., and S. Planton (1989), A simple parameterization of land surface processes for meteorological models, *Mon. Weather Rev.*, *117*, 536–549.

Oleson, K. W., et al. (2013), Technical description of version 4.5 of the Community Land Model (CLM). NCAR Technical Note NCAR/TN-503+STR, 422 pp., National Center for Atmospheric Research, Boulder, Colo., doi:10.5065/D6RR1W7M.

Padro, J. (1996), Summary of ozone dry deposition velocity measurements and model estimates over vineyard, cotton, grass and deciduous forest in summer, *Atmos. Environ.*, *30*(13), 2363–2369.

Pangle, R. E., K. Kavanagh, and R. Duursma (2015), Decline in canopy gas exchange with increasing tree height, atmospheric evaporative demand, and seasonal drought in co-occurring inland Pacific Northwest conifer species, *Can. J. For. Res.*, *45*(8), 1086–1101.

Paw U, K. T., et al. (2004), Carbon dioxide exchange between an old growth forest and the atmosphere, *Ecosystems*, *7*, 513–524.

Phillips, N., B. J. Bond, N. G. McDowell, and M. G. Ryan (2002), Canopy and hydraulic conductance in young, mature and old Douglas-fir trees, *Tree Physiol.*, *22*(2–3), 205–211.

Pisek, J., O. Sonnentag, A. D. Richardson, and M. Mõttus (2013), Is the spherical leaf inclination angle distribution a valid assumption for temperate and boreal broadleaf tree species?, *Agric. For. Meteorol.*, *169*, 186–194.

Pleim, J. E. (2007a), A combined local and nonlocal closure model for the atmospheric boundary layer. Part I: Model description and testing, *J. Appl. Meteorol. Climatol.*, *46*, 1383–1395.

Pleim, J. E. (2007b), A combined local and nonlocal closure model for the atmospheric boundary layer. Part II: Application and evaluation in a mesoscale meteorological model, *J. Appl. Meteorol. Climatol.*, *46*, 1396–1409.

Pleim, J. E., and A. Xiu (1995), Development and testing of a surface flux and planetary boundary layer model for application in mesoscale models, *J. Appl. Meteorol.*, *34*, 16–32.

Pleim, J. E., and A. Xiu (2003), Development of a land surface model. Part II: Data assimilation, *J. Appl. Meteorol.*, *42*, 1811–1822.

Pleim, J. E., and L. Ran (2011), Surface flux modeling for air quality applications, *Atmosphere*, *2*(3), 271–302.

Pleim, J. E., and R. Gilliam (2009), An indirect data assimilation scheme for deep soil temperature in the Pleim-Xiu land surface model, *J. Appl. Meteorol. Climatol.*, *48*, 1362–1376.

Pleim, J. E., A. Xiu, P. L. Finkelstein, and T. L. Otte (2001), A coupled land-surface and dry deposition model and comparison to field measurements of surface heat, moisture, and ozone fluxes, *Water, Air, Soil Pollut.: Focus*, *1*(5–6), 243–252.

Pleim, J. E., J. O. Bash, J. T. Walker, and E. J. Cooter (2013), Development and evaluation of an ammonia bidirectional flux parameterization for air quality models, *J. Geophys. Res. Atmos.*, *118*, 3794–3806.

Pleim, J., R. Gilliam, W. Appel, and L. Ran (2016), *Recent Advances in Modeling of the Atmospheric Boundary Layer and Land Surface in the Coupled WRF-CMAQ Model, Air Pollut. Model. and its Appl. XXIV*, chap. 64, pp. 391–396, Springer International Publishing AG, Cham (ZG), Switzerland.

Qu, W. Q., and A. Henderson-Sellers (1998), Comparing the scatter in PILPS off-line experiments with that in AMIP I coupled experiments, *Global Planet. Change*, *19*, 209–223.

Ran, L., and A. Hanna (2016), Spatial Allocator Version 4.2, the Community Modeling and System analysis at the University of North Carolina, Chapel Hill, NC, 02/05/2016. [Available at https://www.cmascenter.org/sa-tools/documentation/4.2/Raster_Users_Guide_4_2.pdf], Last accessed June 2016.

Ran, L., R. Gilliam, F. S. Binkowski, A. Xiu, J. Pleim, and L. Band (2015), Sensitivity of the weather research and forecast/community multiscale air quality modeling system to MODIS LAI, FPAR, and albedo, *J. Geophys. Res. Atmos.*, *120*, 8491–8511, doi:10.1002/2015JD023424.

Ran, L., J. Pleim, R. Gilliam, F. S. Binkowski, C. Hogrefe, and L. Band (2016), Improved meteorology from an updated WRF/CMAQ modeling system with MODIS vegetation and albedo, *J. Geophys. Res. Atmos.*, *121*, 2393–2415, doi:10.1002/2015JD024406.

Ryan, M. G., and B. J. Yoder (1997), Hydraulic limits to tree height and tree growth, *BioScience*, *47*, 235–242, doi:10.2307/1313077.

Samuelsson, P., B. Bringfelt, and L. P. Graham (2003), The role of aerodynamic roughness for runoff and snow evaporation in land-surface schemes—Comparison of uncoupled and coupled simulations, *Global Planet. Change*, *38*, 93–99.

Sellers, P. J., D. A. Randall, G. J. Collatz, J. A. Berry, C. B. Field, D. A. Dazlich, C. Zhang, G. D. Collelo, and L. Bounoua (1996), A revised land surface parameterization (SiB2) for atmospheric GCMs. Part I: Model formulation, *J. Clim.*, *9*, 676–705.

Shaw, D. C., J. F. Franklin, K. Bible, J. Klopatek, E. Freeman, S. Greene, and G. G. Parker (2004), Ecological setting of the Wind River old-growth forest, *Ecosystems*, *7*(5), 427–439.

Sitch, S., P. M. Cox, W. J. Collins, and C. Huntingford (2007), Indirect radiative forcing of climate change through ozone effects on the land-carbon sink, *Nature*, *448*, 791–794.

Skamarock, W. C., J. B. Klemp, J. Dudhia, D. O. Gill, D. M. Barker, W. Wang, and J. G. Powers (2008), A description of the advanced research WRF version 3, NCAR Tech Note, NCAR/TN 475+STR: 125 pp.

Song, C., G. Katul, R. Oren, L. E. Band, C. L. Tague, P. C. Stoy, and H. R. McCarthy (2009), Energy, water, and carbon fluxes in a loblolly pine stand: Results from uniform and gappy canopy models with comparisons to eddy flux data, *J. Geophys. Res.*, *114*, G04021, doi:10.1029/2009JG000951.

Thomas, S. C., and W. E. Winner (2000), Leaf area index of an old-growth Douglas-fir forest estimated from direct structural measurements in the canopy, *Can. J. For. Res.*, *30*(12), 1922–1930.

Urbanski, S., C. Barford, S. Wofsy, C. Kucharik, E. Pyle, J. Budney, K. McKain, D. Fitzjarrald, M. Czikowsky, and J. W. Munger (2007), Factors controlling CO_2 exchange on timescales from hourly to decadal at Harvard Forest, *J. Geophys. Res.*, *112*, G02020, doi:10.1029/2006JG000293.

Verma, S. B., A. Dobermann, K. G. Cassman, D. T. Walters, J. M. Knops, T. J. Arkebauer, and E. A. Walter-Shea (2005), Annual carbon dioxide exchange in irrigated and rainfed maize-based agroecosystems, *Agric. For. Meteorol.*, *131*(1), 77–96.

Wang, K., and R. E. Dickinson (2012), A review of global terrestrial evapotranspiration: Observation, modeling, climatology, and climatic variability, *Rev. Geophys.*, *50*, RG2005, doi:10.1029/2011RG000373.

Wang, S. X., M. Zhao, J. Xing, Y. Wu, Y. Zhou, Y. Lei, K. B. He, L. X. Fu, and J. M. Hao (2010), Quantifying the air pollutants emission reduction during the 2008 Olympic Games in Beijing, *Environ. Sci. Technol.*, *44*, 2490–2496.

Wang, Y. P., and R. Leuning (1998), A two-leaf model for canopy conductance, photosynthesis and partitioning of available energy. I: Model description and comparison with a multi-layered model, *Agric. For. Meteorol.*, *91*, 89–111, doi:10.1016/S0168-1923(98)00061-6.

Wesely, M. L., and B. B. Hicks (2000), A review of the current status of knowledge on dry deposition, *Atmos. Environ.*, *34*(12), 2261–2282.

Wesely, M. L., J. A. Eastman, D. H. Stedman, and E. D. Yalvac (1982), An eddy correlation measurement of NO_2 flux to vegetation and comparison to O_3 flux, *Atmos. Environ.*, *16*, 815–820.

Wharton, S., M. Schroeder, K. Bible, and M. Falk (2009), Stand-level gas-exchange responses to seasonal drought in very young versus old Douglas-fir forests of the Pacific Northwest, USA, *Tree Physiol.*, *29*(8), 959–974.

Xing, J., R. Mathur, J. Pleim, C. Hogrefe, C.-M. Gan, D. C. Wong, C. Wei, R. Gilliam, and G. Pouliot (2015), Observations and modeling of air quality trends over 1990–2010 across the Northern Hemisphere: China, the United States and Europe, *Atmos. Chem. Phys.*, *15*, 2723–2747, doi:10.5194/acp-15-2723-2015.

Xiu, A., and J. E. Pleim (2001), Development of a land surface model. Part I: Application in a mesoscale meteorological model, *J. Appl. Meteorol.*, *40*, 192–209.

Yang, W., N. V. Shabanov, D. Huang, W. Wang, R. E. Dickinson, R. R. Nemani, Y. Knyazikhin, and R. B. Myneni (2006), Analysis of leaf area index products from combination of MODIS Terra and Aqua data, *Remote Sens. Environ.*, *104*(3), 297–312.

Yu, S., B. Eder, R. Dennis, S. H. Chu, and S. E. Schwartz (2006), New unbiased symmetric metrics for evaluation of air quality models, *Atmos. Sci. Lett.*, *7*(1), 26–34.

Zhang, L., M. D. Moran, and J. R. Brook (2001), A comparison of models to estimate in-canopy photosynthetically active radiation and their influence on canopy stomatal resistance, *Atmos. Environ.*, *35*, 4463–4470.